

Article

Geochemical Characteristics, Palaeoenvironment and Provenance of Uranium-Bearing Sandstone in the Sifangtai Formation, Northern Songliao Basin, Northeast China

Yan Li ^{1,2}, Feng-Jun Nie ^{1,*}, Li-Cheng Jia ³, Sheng-Jun Lu ² and Zhao-Bin Yan ¹

¹ College of Earth Science, East China University of Technology, Nanchang 330013, China; 201800818002@ecut.edu.cn (Y.L.); zbyan@ecit.cn (Z.-B.Y.)

² No. 240 Institute of Nuclear Industry, The China National Nuclear Corporation, Shenyang 110000, China; 13840455361@163.com

³ Beijing Research Institute of Uranium Geology, The China National Nuclear Corporation, Beijing 100029, China; 13717542711@163.com

* Correspondence: niefj@ecit.cn

Abstract: During the Cretaceous period of the northern Songliao Basin (northeast of China), a 100 m thick layer of fluvial-phase sandstone (Sifangtai Formation) with uranium potential was widely deposited, but its geochemical characteristics, palaeoenvironment, and provenance remain unknown. This research proposes a new set of relevant geochemical data for sandstones to investigate their palaeoenvironment, provenance and tectonic setting. The results revealed that: (1) The sandstone of the Sifangtai Formation was dominated by feldspar lithic sandstone. Geochemical signatures demonstrate that these sandstones have a high silicon content ($\text{SiO}_2 = 68.30\sim 83.60$ wt%) and total alkali content, but are poor in magnesium and calcium. They are also enriched in Rb, Th, U, K and LREE, and depleted HFSE (e.g., Nb, Ta), with crustal magmatic source. (2) The paleoclimate discriminant indicated that the rocks of the Sifangtai Formation might that the climate of Sifangtai Formation is semi-arid, and the chemical weathering of the source rocks is weak under the semi-arid climate environment. (3) The combination of element Sr/Ba, $100 \text{ MgO}/\text{Al}_2\text{O}_3$ and the combination of $v/v + \text{Ni}$, V/Cr, Ni/Co, and Sr/Cu indicated that the paleo-water medium was deposited in an oxygen-rich freshwater environment when the Sifangtai Formation was deposited. (4) The discriminate diagrams showed that almost all the sandstones of the Sifangtai Formation fell in the range of the active continental margin, indicating that the source area of the sandstones of Sifangtai Formations is an active continental margin tectonic environment, and the source is a felsic rock developed in the Xiaoxing'an Ridge and Zhangguangcailing area.

Keywords: palaeoenvironment; provenance; geochemical; Sifangtai Formation; northern Songliao Basin



Citation: Li, Y.; Nie, F.-J.; Jia, L.-C.; Lu, S.-J.; Yan, Z.-B. Geochemical Characteristics, Palaeoenvironment and Provenance of Uranium-Bearing Sandstone in the Sifangtai Formation, Northern Songliao Basin, Northeast China. *Minerals* **2021**, *11*, 1019. <https://doi.org/10.3390/min11091019>

Academic Editor: Jaromír Leichmann

Received: 2 August 2021

Accepted: 1 September 2021

Published: 18 September 2021

Publisher's Note: MDPI stays neutral with regard to jurisdictional claims in published maps and institutional affiliations.



Copyright: © 2021 by the authors. Licensee MDPI, Basel, Switzerland. This article is an open access article distributed under the terms and conditions of the Creative Commons Attribution (CC BY) license (<https://creativecommons.org/licenses/by/4.0/>).

1. Introduction

Uranium is an important strategic resource. In particular, sandstone-type uranium deposits are typically targeted during exploration because of the reduced environmental impact and lower mining costs associated with this type of deposit. A number of significant sandstone-hosted uranium deposits are present in the Middle-Cenozoic basins in northern China [1–5]. From east to west, these deposits form the southern region of the Songliao, Erlian, Ordos, and Yili Basins. These basins comprise the Yaojia, Saihan, Zhiluo, and Xishangyao uranium-bearing groups [6–11]. In recent years, two medium-sized deposits have been discovered in the southern region of the basin. These deposits are characterized by significant reserves of uranium resources and show suitable exploration potential [6,7]. Previous studies have investigated the conditions of uranium ore formation, the sedimentary system, the chronology of uranium ore formation, geochemical characteristics, sedimentary diagenesis of ore-bearing sand bodies, the degree of weathering, and the tectonic background [12–15]. These studies have demonstrated that uranium-bearing sandstones of the

Yaojia Formation, which is a part of the Qianjiadian Deposit, were likely derived from acidic volcanic rocks and granites from ancient uplift around the basin [6]. Moreover, the Yaojia Formation is characterized by four types of sedimentary phases during the depositional period: alluvial fan, river, delta, and lake, and fluvial deposits in this formation are related to uranium mineralization [16,17]. Finally, the provenance of Yaojia Formation sandstone in the Kailu Depression of the Qianjiadian Deposit were formed in a passive continental margin environment and were predominately derived from a volcanic-sedimentary rock system in the northern margin of the North China Craton [6,7,18].

However, most studies have focused on the southern region of the Songliao Basin, and its northern region has not been extensively studied. Increased exploration and research in recent years have resulted in several uranium industrial and mineralized drills in the Sifangtai Formation, and these have revealed the significant uranium mineralization potential of this formation [16]. However, the geochemical characteristics, paleoenvironment, and provenance of the Sifangtai Formation remain unclear. Therefore, the relationship between the Sifangtai Formation sandstone and uranium mineralization in the area cannot be accurately discerned, severely limiting uranium prospecting in the region.

Sedimentary geochemistry is an indispensable tool for constraining the geological environment associated with sandstone-bearing uranium mineralization, such as the paleoenvironment, plate movement, and crustal evolution [17–22]. Trace elements and their sedimentary contents record paleoenvironmental and paleoclimatic changes and can be used to constrain the physical origin of sedimentary basins, tectonic background of source areas, and relationship between orogenic processes and basin development [23–25]. In this study, we aimed to reconstruct the depositional environment (host rock type, provenance, paleoweathering, and paleoclimate) of the uranium-bearing Sifangtai Formation in the Nenjiang–Fuyu area of northern Songliao Basin by investigating the whole-rock geochemistry of this formation as well as geochemical data obtained by various testing methods to generate a reference for the exploration and development of this mineral resource.

2. Geological Setting and Sample Descriptions

The Songliao Basin is a large Miocene oil, gas and uranium-bearing basin in the northeastern region of China [26–29]. The basin has a rhombus shape and covers an area of 260,000 km² (Figure 1). The Songliao Basin is surrounded by the following mountain ranges: the Lesser Xing'an Range to the northeast, the Great Xing'an Range in the northwest, the Zhangguangcai Range to the east, and the North China Craton in the south (Figure 1). The basement of the basin predominately comprises pre-Paleogene and Paleozoic metamorphic and Late Paleozoic Era granites and amphibolites [26–28]. Moreover, the Songliao Basin basement rocks are exposed around the basin and serve as the parent rocks for the Mesozoic sedimentary rocks in the basin. The sedimentary cover of the upper region of the basin is mainly composed of Middle Cenozoic sedimentary rocks. Sediments from the Upper-Late Cretaceous, Huoshiling (K₁hs), Shahezi (K₁sh) and Yingcheng (K₁yc) formations were fracture phase. During this period, the subduction of the Pacific plate led to the thermal expansion of upper mantle material, and the study area entered a stage of extensional subsidence development, forming a group of independently spreading semi-graben and graben-type subsidence basins [30]. The Quantou (K₂q), Qingshankou (K₂qn), Yaojia (K₂y), and Nenjiang (K₂n) formations formed from the post-rift thermal subsidence of the basin (Figure 2). After the conclusion of fracture deposition, the study area entered a stage of thermal cooling depression development. The depositional environment and sedimentary phase system in this period were typically characterized by overburden in the west and a large, long-axis fluvial-deltaic sedimentary system in the northern region of the Songliao Basin [30,31]. The Sifangtai (K₂s) and Mingshui (K₂m) formations formed during the basin shrinkage stage [31–33]. Due to strengthening of the subducting Pacific Plate and the extrusion of the peripheral plate, the basin shows significant fold reversal and retrograde reversal fractures. The sediments are mainly distributed in the middle and western regions of the basin, and the fluvial phase is well developed. The Nenjiang

Formation was subjected to significant denudation in the northern region of the basin, and it formed a series of denudation tectonic skylights [32,33]. The Sifangtai Formation of the uranium ore-bearing layer developed from north to south in the sequence of alluvial fan, river, delta, and lake deposits, with narrow spreading and thickness of approximately 100 m (Figure 3b,c).

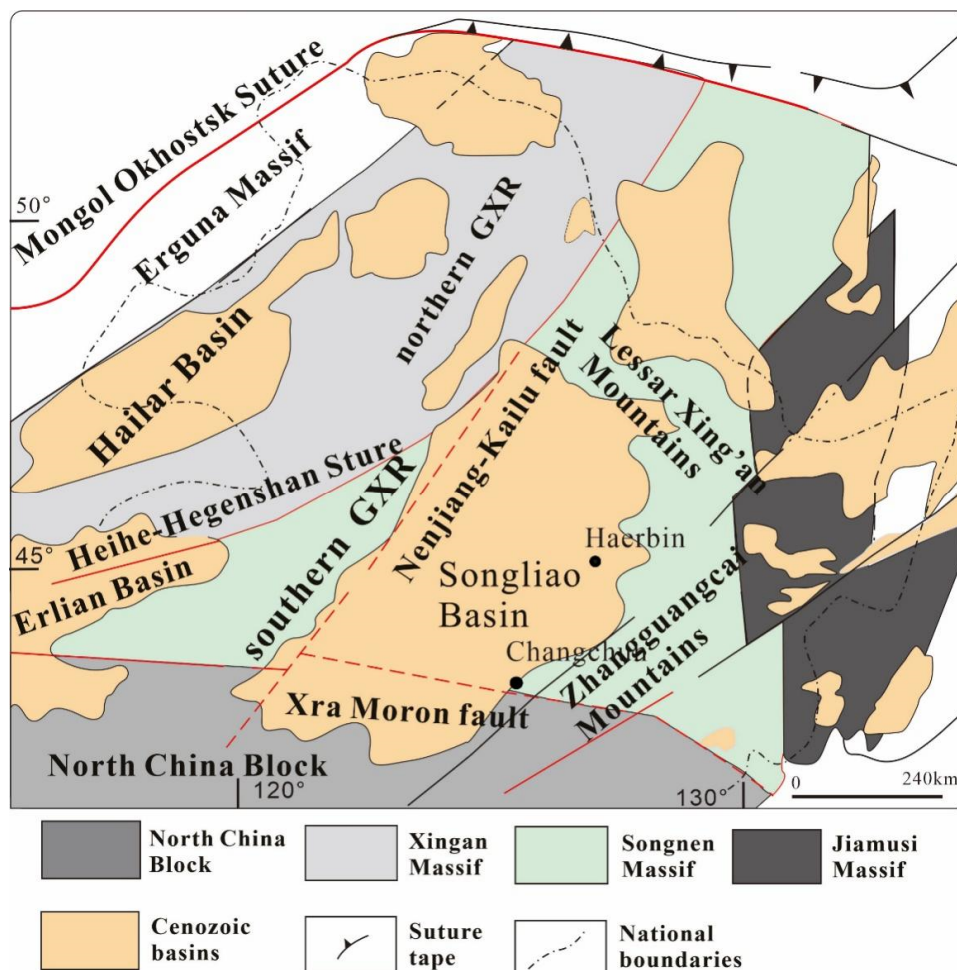


Figure 1. Sketch geological map of northeastern China (after [29,30]). GXR, Great Xing'an Range.

The study area is situated in northern Songliao Basin (Figure 3a), and uranium is hosted in the Sifangtai Formation, which is located 300–500 m below the surface. The ore-hosting sediments are mainly composed of fine-grained sandstone with a massive structure. The sandstone units are angular and predominately composed of plagioclase (15–20 vol.%), quartz (40–50 vol.%), potassium feldspar (10–15 vol.%), and trace amounts of rock debris (15–20 vol.%). The cement comprises clay minerals (Figure 4), and the Sifangtai formation was presumably formed by proximal deposition.

The minerals associated with uranium in the study area are mainly star-shaped pyrite and organic matter derived from plant charcoal debris. Overall, this area of tectonic evolution has undergone four stages: Early Cretaceous faulting, Late Early Cretaceous uplift denudation, Late Cretaceous depression, and tectonic inversion and uplift denudation. The tectonic inversion represents the recharge area for groundwater and a discharge area for groundwater within the aquifer, and these conditions are extremely favorable for uranium ore formation [34–36].

		mem ber	Formation	Thick ness	Lithological characteristics	Sedimentary phase	Paleoclima te conditions	Geochemical environment	Tectonic Evolution
Quaternary		Q		60–210		diluvium	warm and humid	Oxidation	
Neogene	upper Neogene	N ₂ t	Taikang Formation	31–72		meandering river	warm and humid	weak reduction	Difference lifting and lowering
	lower Neogene	N ₁ d	Daan Formation	21–98		meandering–braided river	semi arid	weak reduction	
Cretaceous	upper Cretaceous	K ₂ m	Mingshui Formation	0–155		diluvium–river	warm and humid	weak reduction	Shrinking stage
		K ₂ s	Sifangtai Formation	30–249		alluvial fan river delta lake	arid–semi arid	Oxidation	
		K ₂ n	Nenjiang Formation	34–240		shallow lake half deep lake	warm and humid	weak reduction–Oxidation	post–rift subsidence
		K ₂ y	Yaojia Formation	70–190		alluvial fan river shallow lake	semi–arid	Oxidation	
		K ₂ qn	Qingshan kou Formation	80–100		river shallow lake half deep lake	warm and humid	weak reduction–Oxidation	
		K ₂ q	Quantou Formation	90–500		river	arid	Oxidation	
	lower Cretaceous	K ₁ d	Denglou ku Formation	680		shallow lake delta	semi–arid	weak reduction–Oxidation	fracture phase
		K ₁ y	Yingcheng Formation	624		half deep lake shallow lake	warm and humid	reduction	
		K ₁ s	Shahezi Formation	1108		half deep lake shallow lake	semi–arid	reduction	
		K ₁ h	Huoshi ling Formation	248.3		lake	semi–arid	weak reduction–Oxidation	
Carboniferous–Permian		C–P		unclear					
Sinian Syste		AnZ		unclear					

Figure 2. Stratigraphic sketch of the northern part of Songliao Basin.

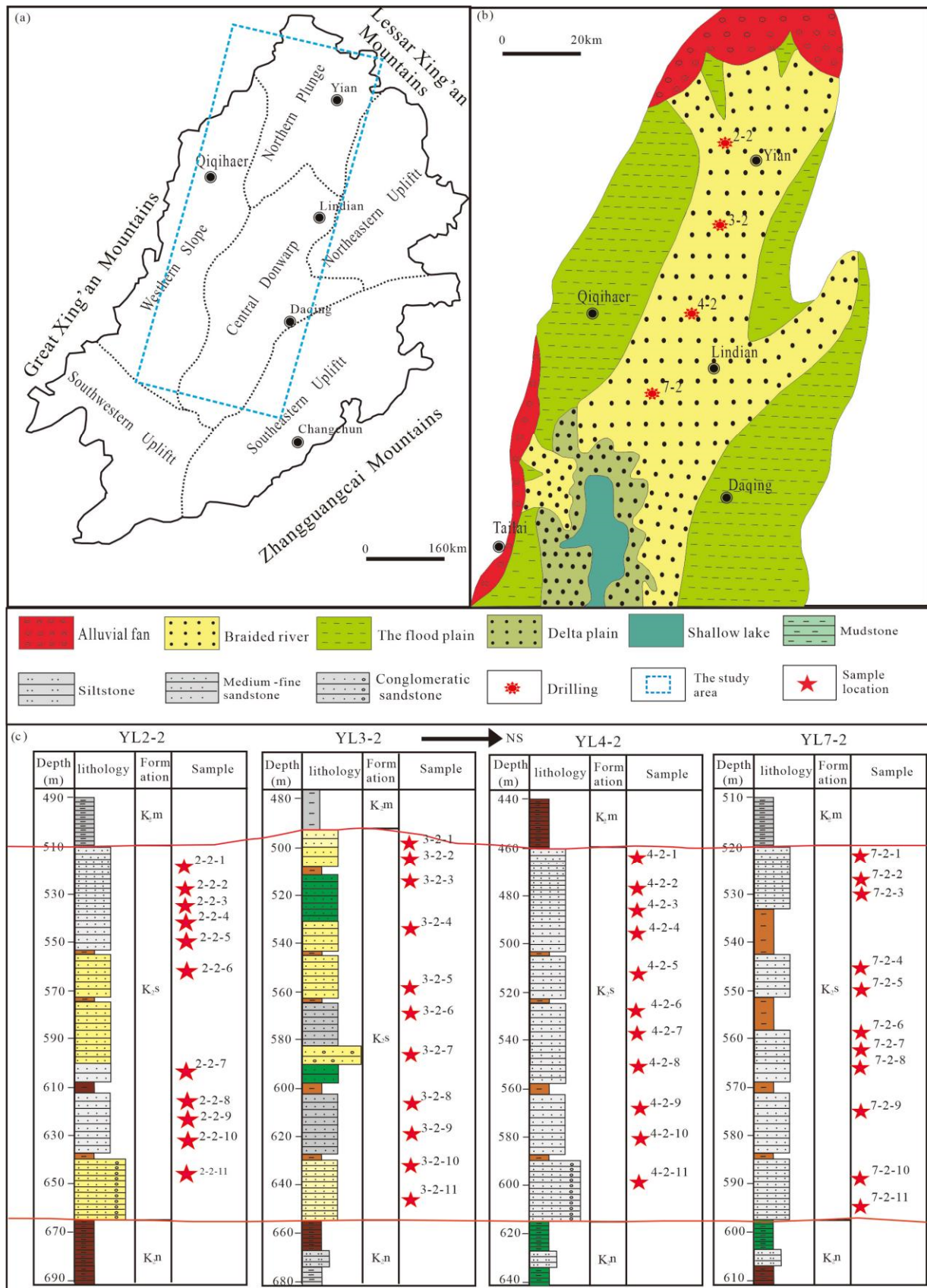


Figure 3. (a) Structural partition map, (b) sedimentary phase diagram of the Sifangtai Group, (c) drilling sampling map of the study area.

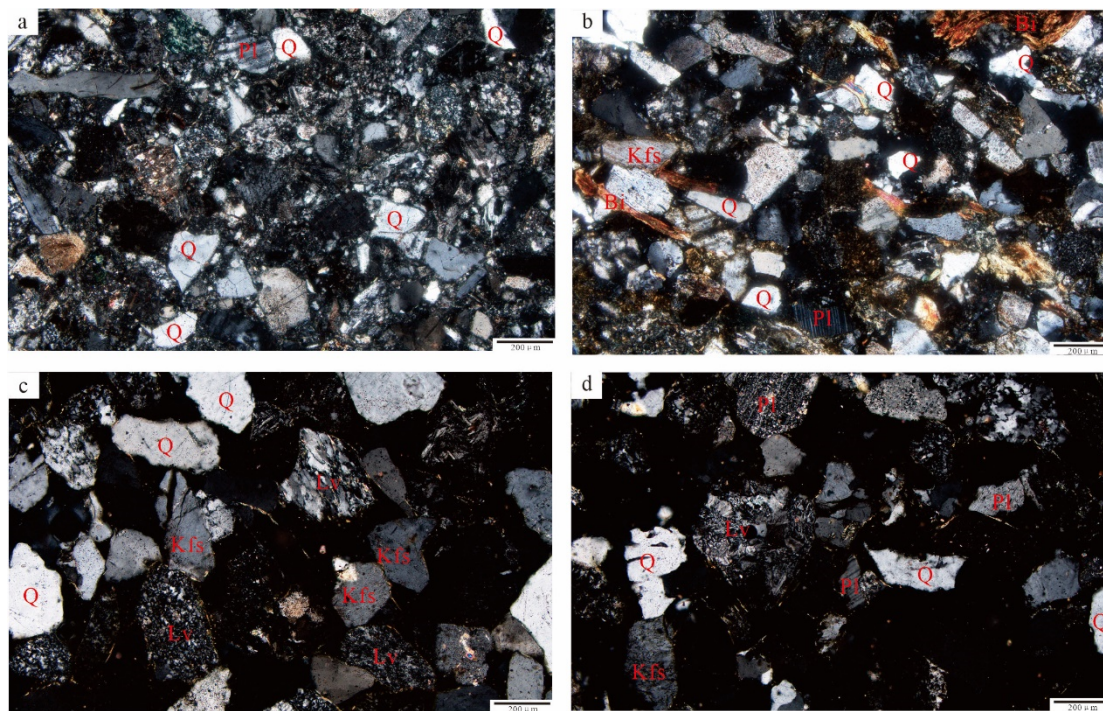


Figure 4. Micrographs of sandstones in northern Songliao Basin. (a–d) Grey sandstone of the Sifangtai Formation Q—Quartz, Pl—plagioclase, Kfs—potassium feldspar, Bi—Biotite, Lv—Debris.

3. Analytical Methods

Elemental geochemical data were determined by the Beijing Research Institute of Uranium Geology (Beijing, China), CNNC (Beijing, China). Major elements were tested using XRF analysis with a relative error of less than 5%, and trace and rare earth elements (REEs) were analyzed using a Perkin Elmer Elan 6100 DRC inductively coupled plasma mass spectrometer (ICP-MS) (Perkin Elmer, Waltham, MA, USA). The sample analysis was monitored using reference materials AVG-1 and BHVO-1, and the relative error was generally less than 5% [37].

4. Analytical Results

4.1. Major Elements

The sandstones in the northern Songliao Basin had a high SiO_2 content range of 68.30–83.60 wt%, with an average value of 77.70 wt%. The total alkali ($\text{Na}_2\text{O} + \text{K}_2\text{O}$) content ranged from 4.24 wt% to 7.03 wt%, with an average value of 5.89 wt%. The rocks also had a high aluminum content ($\text{Al}_2\text{O}_3 = 8.71\text{--}15.06$ wt%) and low magnesium and calcium content ($\text{MgO} = 0.12\text{--}1.38$ wt%; $\text{CaO} = 0.35\text{--}1.07$ wt%).

With respect to the $\text{SiO}_2\text{--Al}_2\text{O}_3$ plot, most of the sandstones were plotted in the plagioclase, potassium feldspar, and quartz regions (Figure 5a), whereas for the $\log(\text{SiO}_2/\text{Al}_2\text{O}_3)\text{--}\log(\text{TFe}_2\text{O}_3/\text{K}_2\text{O})$ plot, all the sandstones were plotted in the feldspar sandstone region (Figure 5b). Overall, the trace amounts of MnO and P_2O_5 detected in the samples suggest the presence of heavy minerals, such as apatite and chlorite, in the rocks of this area.

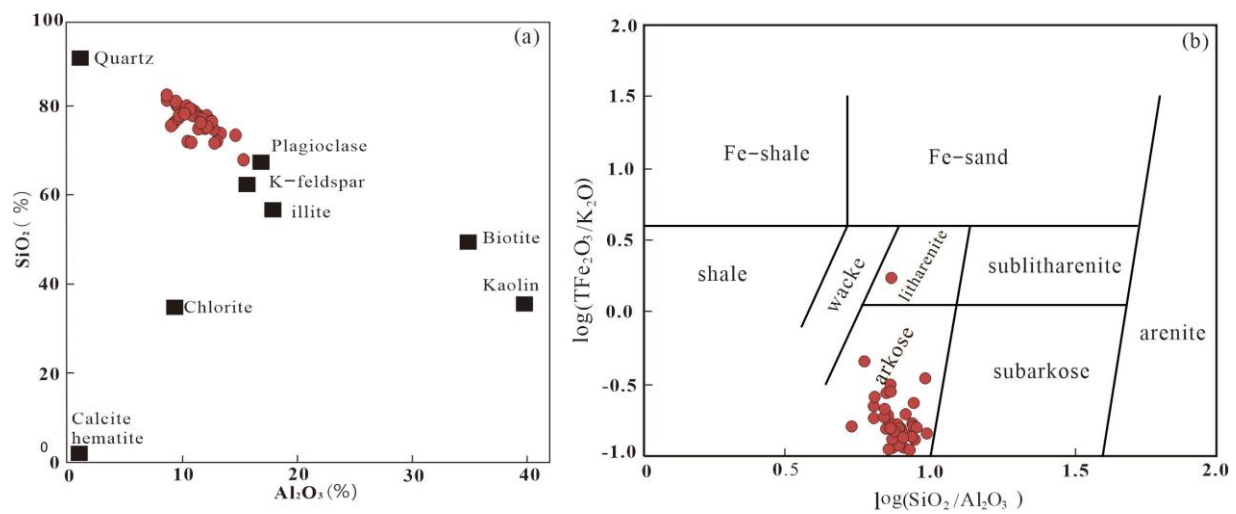


Figure 5. Diagram of the sandstones (a) and $\log(\text{SiO}_2/\text{Al}_2\text{O}_3) - \log(\text{TFe}_2\text{O}_3/\text{K}_2\text{O})$ diagram (b) (after Herro et al. [38]).

4.2. Trace and Rare Earth Elements

Chondrite-normalized REE patterns revealed similar patterns for all the sandstone samples ($\Sigma\text{REE} = 65.54\text{--}283.55$ ppm, with an average value of 105.27 ppm). Moreover, the REE distribution pattern was right-inclined (Figure 6a), with relatively enriched light rare earth elements (LREEs) and depleted heavy rare earth elements (HREEs). The LREE and HREE ratios ranged from 6.89 to 12.90. Moreover, the fractionation coefficients ranged from 2.95 to 5.35 for the LREEs $(\text{La}/\text{Sm})_{\text{N}}$ and from 1.09 to 2.24 for the HREEs $(\text{Gd}/\text{Yb})_{\text{N}}$, with a more substantial trend of LREE fractionation than HREE fractionation. A weak Eu negative anomaly ($\delta\text{Eu} = 0.57\text{--}1.00$), which was slightly higher than PAAS (0.65) and closer to UCC (0.70), was detected, indicating that the sandstone host rock was derived from rocks of the upper crust.

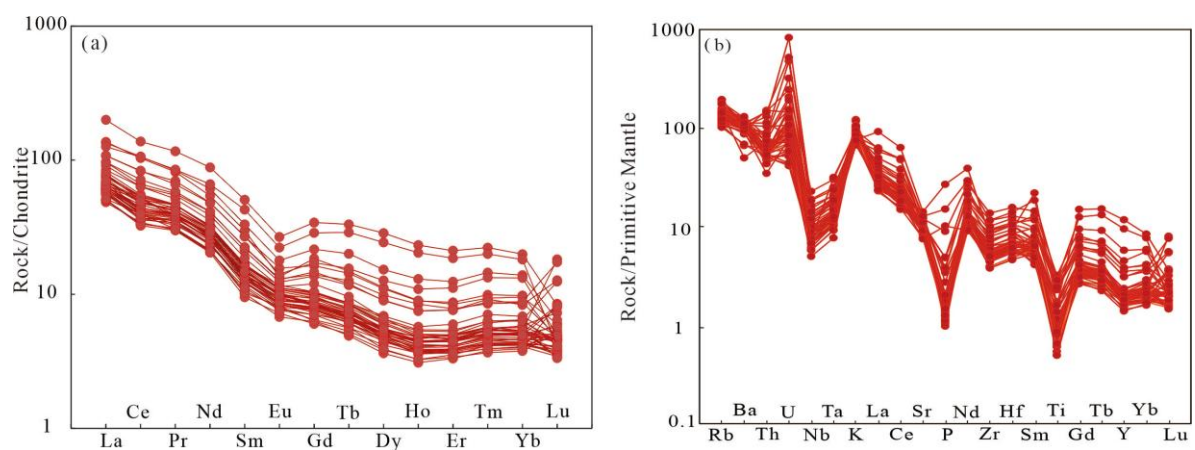


Figure 6. Chondrite normalized REE patterns (a) and primitive mantle normalized trace element spider diagrams (b) for the Sandstones in northern Songliao Basin (after Sun, S.S. and McDonough. [39]).

The primitive mantle-normalized spider diagram indicated a consistent evolutionary trend for all the samples (Figure 6b) characterized by the enrichment of large-ion lithophile elements (e.g., Rb, Th and U), strong depletion of Sr, P, and Ti, and a relative depletion of Nb and Ta (Table 1).

Table 1. Geochemical analysis of sandstone in the Sifangtai Formation.

No	SampleNo.	SiO ₂	TiO ₂	Al ₂ O ₃	TFe ₂ O ₃	MnO	CaO	MgO	Na ₂ O	K ₂ O	P ₂ O ₅	LOI	TOTAL	Na ₂ O +K ₂ O	SiO ₂ / Al ₂ O ₃	Na ₂ O +Ca ₂ O	100MgO/ Al ₂ O ₃	CIA	ICV
1	Y4-2-1	74.52	0.26	13.16	0.65	0.03	0.54	0.35	3.05	3.52	0.02	2.94	99.04	6.57	5.66	3.59	2.68	56.13	0.64
2	Y4-2-2	78.04	0.18	11.45	0.35	0.02	0.48	0.26	2.80	3.28	0.02	2.25	99.13	6.08	6.82	3.28	2.29	54.75	0.64
3	Y4-2-3	82.46	0.13	8.72	1.03	0.03	0.38	0.21	2.10	2.69	0.02	1.55	99.32	4.79	9.46	2.48	2.42	54.18	0.75
4	Y4-2-4	81.24	0.20	9.53	0.35	0.02	0.62	0.17	2.42	2.81	0.03	1.49	98.87	5.23	8.52	3.04	1.75	52.86	0.69
5	Y4-2-5	72.65	0.50	12.86	0.65	0.06	0.84	0.60	2.38	2.83	0.05	4.46	97.88	5.21	5.65	3.22	4.68	59.40	0.61
6	Y4-2-6	79.38	0.22	11.00	0.50	0.02	0.55	0.22	2.95	3.22	0.02	1.41	99.49	6.17	7.22	3.50	1.95	52.89	0.70
7	Y4-2-7	78.82	0.23	11.31	0.50	0.01	0.60	0.23	3.05	3.32	0.05	1.46	99.57	6.37	6.97	3.65	2.00	52.81	0.70
8	Y4-2-8	80.39	0.18	10.57	0.35	0.01	0.51	0.16	2.83	3.26	0.03	1.30	99.59	6.09	7.61	3.34	1.54	52.60	0.69
9	Y4-2-9	75.56	0.37	12.57	0.30	0.02	0.64	0.33	3.24	3.46	0.03	2.04	98.55	6.70	6.01	3.88	2.60	53.96	0.66
10	Y4-2-10	79.38	0.15	10.74	0.50	0.01	0.53	0.28	2.90	3.26	0.02	1.81	99.58	6.16	7.39	3.43	2.59	52.47	0.71
11	Y4-2-11	78.89	0.17	11.01	0.55	0.02	0.53	0.27	3.00	3.34	0.01	1.78	99.57	6.34	7.17	3.53	2.47	52.39	0.71
12	Y3-2-1	79.18	0.24	10.87	0.44	0.01	0.41	0.20	2.81	3.34	0.02	1.64	99.15	6.15	7.28	3.22	1.88	53.56	0.68
13	Y3-2-2	79.74	0.20	11.01	0.40	0.01	0.41	0.15	3.03	3.59	0.02	1.32	99.87	6.62	7.24	3.44	1.40	52.17	0.71
14	Y3-2-3	80.16	0.17	10.78	0.50	0.01	0.39	0.20	2.68	3.39	0.02	1.46	99.76	6.07	7.44	3.07	1.85	53.93	0.68
15	Y3-2-4	78.82	0.20	10.84	0.50	0.02	0.44	0.24	2.71	3.28	0.02	2.38	99.45	5.99	7.27	3.15	2.24	53.98	0.68
16	Y3-2-5	80.93	0.20	9.74	0.49	0.01	0.43	0.21	2.59	2.93	0.02	1.40	98.95	5.52	8.31	3.02	2.13	53.07	0.70
17	Y3-2-6	81.02	0.19	9.66	0.50	0.01	0.39	0.17	2.56	3.16	0.02	1.60	99.29	5.72	8.39	2.95	1.73	52.51	0.72
18	Y3-2-7	75.74	0.24	11.85	0.50	0.03	0.56	0.31	3.18	3.29	0.03	2.22	97.95	6.47	6.39	3.74	2.62	53.52	0.68
19	Y3-2-8	82.13	0.17	9.47	0.45	0.01	0.41	0.16	2.64	2.90	0.02	1.41	99.77	5.54	8.67	3.05	1.67	52.32	0.71
20	Y3-2-9	83.60	0.13	8.71	0.39	0.01	0.35	0.14	2.45	2.80	0.02	1.18	99.77	5.25	9.60	2.80	1.62	51.92	0.72
21	Y3-2-10	78.25	0.19	11.52	0.44	0.02	0.45	0.25	3.09	3.51	0.02	1.48	99.22	6.6	6.79	3.54	2.20	53.07	0.69
22	Y3-2-11	81.02	0.12	10.34	0.44	0.01	0.36	0.12	2.96	3.28	0.02	1.03	99.69	6.24	7.84	3.32	1.15	51.99	0.70
23	Y2-2-1	78.75	0.38	12.01	0.50	0.04	0.93	0.33	3.12	2.82	0.04	0.60	99.52	5.94	6.56	4.05	2.76	53.78	0.67
24	Y2-2-2	77.07	0.35	11.84	0.65	0.03	0.59	0.26	3.09	3.34	0.02	1.97	99.21	6.43	6.51	3.68	2.19	53.59	0.70
25	Y2-2-3	77.11	0.11	9.32	0.40	0.01	0.40	0.19	2.41	3.07	0.02	1.04	94.07	5.48	8.27	2.81	2.03	52.65	0.71
26	Y2-2-4	72.62	0.30	10.43	0.45	0.02	0.50	0.19	2.98	3.10	0.02	1.22	91.83	6.08	6.96	3.48	1.78	52.00	0.72
27	Y2-2-5	72.39	0.22	10.74	5.43	1.66	0.52	0.48	2.19	2.23	0.03	3.47	99.35	4.42	6.74	2.71	4.43	59.61	1.03
28	Y2-2-6	76.91	0.25	12.28	0.65	0.02	0.54	0.20	3.35	3.46	0.02	1.61	99.27	6.81	6.26	3.89	1.59	53.30	0.69
29	Y2-2-7	76.39	0.36	11.90	0.85	0.02	0.88	0.68	2.45	2.90	0.07	3.03	99.53	5.35	6.42	3.33	5.71	56.87	0.68
30	Y2-2-8	75.66	0.55	11.33	0.94	0.02	0.87	0.60	2.42	2.75	0.07	2.55	97.77	5.17	6.68	3.29	5.33	56.30	0.72
31	Y2-2-9	76.93	0.18	11.73	0.42	0.01	0.37	0.20	2.77	4.04	0.02	1.65	98.32	6.81	6.56	3.14	1.73	53.86	0.68
32	Y2-2-10	76.39	0.25	9.07	0.59	0.04	0.94	0.93	1.82	2.42	0.15	6.53	99.12	4.24	8.42	2.76	10.21	55.47	0.77
33	Y2-2-11	77.89	0.20	11.65	0.60	0.02	0.39	0.24	2.79	3.91	0.02	1.60	99.30	6.7	6.69	3.18	2.03	53.90	0.70
34	Y7-2-1	68.30	0.69	15.06	0.50	0.02	0.76	1.06	2.82	3.16	0.13	1.88	94.38	5.98	4.54	3.58	7.04	61.02	0.60
35	Y7-2-2	78.13	0.14	9.68	0.30	0.01	0.39	0.17	2.86	3.03	0.02	1.97	96.70	5.89	8.07	3.25	1.75	51.44	0.71
36	Y7-2-3	77.36	0.36	12.42	0.35	0.02	0.52	0.24	3.49	3.54	0.03	1.04	99.37	7.03	6.23	4.01	1.96	52.91	0.69
37	Y7-2-4	77.35	0.30	12.42	0.25	0.01	0.54	0.27	3.48	3.48	0.03	1.22	99.33	6.96	6.23	4.02	2.15	53.03	0.67
38	Y7-2-5	78.76	0.18	9.73	0.30	0.01	0.39	0.25	2.60	2.92	0.03	4.47	99.63	5.52	8.09	2.99	2.57	53.29	0.68
39	Y7-2-6	80.38	0.19	10.61	0.40	0.01	0.47	0.28	2.89	3.10	0.02	1.61	99.96	5.99	7.58	3.36	2.67	53.01	0.69
40	Y7-2-7	79.20	0.34	10.19	0.50	0.17	0.53	0.65	2.31	2.52	0.38	3.03	99.83	4.83	7.77	2.84	6.40	59.37	0.67
41	Y7-2-8	72.27	0.49	12.66	0.75	0.02	0.97	0.89	2.83	2.75	0.03	2.55	96.21	5.58	5.71	3.80	7.05	56.34	0.69
42	Y7-2-9	76.08	0.53	12.07	0.60	0.02	0.90	0.66	2.88	2.75	0.03	1.65	98.17	5.63	6.30	3.78	5.50	55.26	0.69
43	Y7-2-10	74.10	0.62	14.39	1.46	0.03	0.77	0.46	2.48	2.79	0.06	2.53	99.69	5.27	5.15	3.25	3.20	62.07	0.60
44	Y7-2-11	77.04	0.62	11.52	0.75	0.05	1.07	1.38	2.73	2.50	0.22	1.60	99.47	5.23	6.69	3.80	11.98	55.87	0.79

Table 1. Cont.

No.	SampleNo.	PIA	La	Ce	Pr	Nd	Sm	Eu	Gd	Tb	Dy	Ho	Er	Tm	Yb	Lu	Y	ΣREE	LREE	HREE	LREE/HREE
1	Y4-2-1	59.08	17.70	32.00	3.79	13.90	2.35	0.58	1.98	0.31	1.69	0.33	0.97	0.18	1.12	0.11	9.24	77.00	70.32	6.68	10.53
2	Y4-2-2	57.19	15.30	27.90	3.42	12.50	2.04	0.57	1.67	0.28	1.47	0.28	0.83	0.14	0.97	0.12	7.90	67.49	61.73	5.76	10.71
3	Y4-2-3	56.54	15.80	27.20	3.50	12.60	1.94	0.49	1.62	0.24	1.18	0.23	0.71	0.12	0.81	0.27	6.31	66.71	61.53	5.18	11.87
4	Y4-2-4	54.31	20.20	34.10	4.50	16.60	2.71	0.71	2.22	0.34	1.63	0.28	0.82	0.14	0.88	0.12	7.61	85.23	78.82	6.42	12.29
5	Y4-2-5	63.11	34.00	67.30	7.92	28.80	5.17	1.13	4.23	0.70	3.57	0.66	1.85	0.32	2.03	0.15	17.20	157.83	144.32	13.51	10.68
6	Y4-2-6	54.35	16.00	26.40	3.39	12.20	1.82	0.52	1.56	0.25	1.25	0.24	0.75	0.13	0.91	0.12	6.95	65.54	60.33	5.21	11.58
7	Y4-2-7	54.23	18.00	30.00	4.13	15.80	2.50	0.62	2.04	0.32	1.64	0.31	0.88	0.16	0.98	0.19	8.43	77.57	71.05	6.52	10.90
8	Y4-2-8	54.01	17.70	29.20	3.87	14.20	2.32	0.61	1.90	0.30	1.50	0.27	0.81	0.14	0.87	0.12	7.42	73.80	67.90	5.90	11.52
9	Y4-2-9	55.84	24.40	41.30	5.24	19.20	3.22	0.80	2.62	0.43	2.14	0.40	1.15	0.20	1.34	0.13	10.50	102.58	94.16	8.41	11.19
10	Y4-2-10	53.77	19.30	34.50	4.33	16.50	2.56	0.69	2.13	0.33	1.53	0.28	0.79	0.13	0.86	0.16	7.23	84.08	77.88	6.20	12.55
11	Y4-2-11	53.65	18.80	33.60	4.28	17.10	2.59	0.75	2.16	0.33	1.59	0.29	0.83	0.14	0.90	0.13	7.76	83.49	77.12	6.37	12.11
12	Y3-2-1	55.53	21.00	39.10	4.75	18.30	2.90	0.70	2.29	0.37	1.74	0.33	0.94	0.16	1.08	0.16	8.65	93.82	86.75	7.07	12.27
13	Y3-2-2	53.43	19.60	37.80	4.51	16.20	2.69	0.72	2.13	0.33	1.59	0.30	0.89	0.15	0.95	0.15	8.39	88.01	81.52	6.49	12.56
14	Y3-2-3	56.21	21.90	42.10	4.96	18.50	3.00	0.76	2.44	0.39	1.94	0.36	1.04	0.17	1.12	0.14	9.99	98.82	91.22	7.61	11.99
15	Y3-2-4	56.16	23.60	42.90	5.23	19.40	3.17	0.78	2.52	0.37	1.83	0.33	0.98	0.16	1.07	0.15	8.79	102.49	95.08	7.41	12.83
16	Y3-2-5	54.69	19.30	35.70	4.43	16.80	2.58	0.66	2.18	0.34	1.66	0.31	0.88	0.16	1.04	0.14	8.32	86.19	79.47	6.71	11.84
17	Y3-2-6	54.00	21.70	40.00	4.76	17.80	2.93	0.73	2.40	0.37	1.77	0.33	0.95	0.16	1.02	0.13	8.85	95.03	87.92	7.12	12.35
18	Y3-2-7	55.19	16.00	27.20	3.52	12.80	1.96	0.59	1.64	0.26	1.36	0.27	0.82	0.14	0.91	0.11	7.70	67.59	62.07	5.52	11.25
19	Y3-2-8	53.55	19.60	32.40	4.19	15.30	2.38	0.60	1.98	0.30	1.44	0.28	0.83	0.14	0.89	0.13	7.54	80.45	74.47	5.98	12.45
20	Y3-2-9	53.00	20.20	35.80	4.51	15.80	2.63	0.64	2.25	0.32	1.47	0.27	0.78	0.13	0.85	0.11	7.07	85.75	79.58	6.17	12.90
21	Y3-2-10	54.73	20.50	34.50	4.44	16.20	2.52	0.65	2.20	0.33	1.54	0.30	0.86	0.15	0.95	0.16	8.12	85.29	78.81	6.49	12.15
22	Y3-2-11	53.10	18.70	30.00	4.00	14.20	2.22	0.57	1.82	0.28	1.27	0.24	0.72	0.12	0.78	0.17	6.51	75.09	69.69	5.40	12.90
23	Y2-2-1	55.21	23.10	38.40	4.96	18.30	3.08	0.78	2.56	0.41	2.00	0.37	1.06	0.18	1.17	0.11	9.28	96.48	88.62	7.85	11.28
24	Y2-2-2	55.34	21.10	35.60	4.52	17.00	2.72	0.66	2.24	0.36	1.78	0.36	1.04	0.18	1.20	0.15	9.53	88.90	81.60	7.30	11.18
25	Y2-2-3	54.24	18.30	31.30	3.99	13.80	2.38	0.61	1.98	0.30	1.53	0.28	0.77	0.13	0.83	0.17	7.37	76.37	70.38	5.99	11.75
26	Y2-2-4	53.00	18.90	32.40	3.97	15.00	2.47	0.63	2.08	0.33	1.77	0.35	0.99	0.17	1.11	0.15	9.30	80.32	73.37	6.96	10.54
27	Y2-2-5	63.12	18.80	33.20	4.28	15.40	2.60	0.62	2.09	0.35	1.80	0.35	1.00	0.18	1.21	0.24	9.74	82.11	74.90	7.22	10.38
28	Y2-2-6	54.89	17.40	30.10	3.72	14.40	2.33	0.63	2.00	0.32	1.61	0.33	0.94	0.17	1.08	0.27	8.93	75.29	68.58	6.72	10.21
29	Y2-2-7	59.82	30.30	54.00	6.38	24.60	4.30	0.94	3.63	0.62	3.20	0.62	1.66	0.27	1.80	0.16	16.00	132.49	120.52	11.96	10.07
30	Y2-2-8	58.95	43.10	84.30	9.25	32.40	5.72	0.97	4.79	0.73	3.64	0.67	1.79	0.30	1.98	0.19	17.40	189.83	175.74	14.09	12.47
31	Y2-2-9	56.44	19.40	42.10	4.28	15.40	2.60	0.73	2.13	0.35	1.74	0.33	0.98	0.16	1.06	0.15	8.49	91.41	84.51	6.89	12.26
32	Y2-2-10	58.05	16.20	32.30	3.47	12.40	2.15	0.55	1.83	0.31	1.67	0.34	1.06	0.20	1.34	0.40	10.70	74.22	67.07	7.15	9.38
33	Y2-2-11	56.41	20.60	42.40	4.45	16.50	2.79	0.74	2.20	0.35	1.71	0.32	0.98	0.16	1.02	0.15	8.41	94.37	87.48	6.89	12.70
34	Y7-2-1	65.24	42.30	86.50	9.48	36.50	6.36	1.29	5.61	0.98	4.96	0.96	2.64	0.47	2.88	0.21	26.10	201.14	182.43	18.71	9.75
35	Y7-2-2	52.21	24.40	44.10	5.27	19.40	3.13	0.81	2.67	0.41	1.95	0.36	0.98	0.16	1.05	0.18	8.95	104.87	97.11	7.77	12.51
36	Y7-2-3	54.32	25.80	45.10	5.30	18.80	3.12	0.84	2.70	0.42	2.24	0.42	1.27	0.23	1.42	0.16	10.60	107.82	98.96	8.86	11.17
37	Y7-2-4	54.46	24.70	43.10	5.23	18.90	3.07	0.80	2.70	0.42	2.05	0.39	1.12	0.20	1.31	0.14	9.75	104.14	95.80	8.34	11.49
38	Y7-2-5	55.03	26.60	51.60	5.83	21.20	3.56	0.82	3.10	0.47	2.15	0.37	1.06	0.18	1.11	0.59	9.13	118.65	109.61	9.04	12.13
39	Y7-2-6	54.53	22.10	40.00	4.69	17.30	2.83	0.71	2.43	0.38	1.79	0.32	0.95	0.17	1.03	0.26	8.23	94.96	87.63	7.33	11.96
40	Y7-2-7	63.74	62.90	112.00	13.20	52.70	9.70	1.93	8.88	1.63	9.29	1.72	4.49	0.72	4.13	0.27	53.20	283.55	252.43	31.12	8.11
41	Y7-2-8	58.63	28.70	51.60	6.20	23.20	4.04	0.89	3.54	0.57	2.94	0.56	1.62	0.30	1.73	0.41	14.20	126.30	114.63	11.67	9.82
42	Y7-2-9	57.24	30.50	58.20	6.62	24.70	4.28	0.93	3.80	0.59	2.92	0.56	1.62	0.28	1.82	0.56	14.00	137.37	125.23	12.14	10.31
43	Y7-2-10	66.33	34.10	67.80	7.49	28.60	5.19	1.02	4.46	0.76	4.12	0.81	2.37	0.43	2.75	0.16	20.40	160.06	144.20	15.86	9.09
44	Y7-2-11	57.95	39.70	85.90	9.64	39.50	8.20	1.61	7.44	1.42	7.92	1.51	3.95	0.64	3.77	0.13	43.00	211.33	184.55	26.78	6.89

Table 1. Cont.

No.	SampleNo.	La _N /Yb _N	La _N /Sm _N	Gd _N /Yb _N	δEu	δCe	Rb	Ba	Th	U	Nb	Ta	Sr	Zr	Hf	V	Co	Cu	Cr	Ti
1	Y4-2-1	11.34	4.58	1.42	0.82	0.96	106	776	6.14	1.75	7.08	0.592	238	81.6	2.64	24.80	3.02	6.20	9.12	1556
2	Y4-2-2	11.37	4.56	1.39	0.94	0.95	98.3	756	4.84	1.47	5.35	0.46	225	64.8	2.21	17.60	1.24	4.75	8.06	1101
3	Y4-2-3	13.96	4.96	1.60	0.84	0.90	71.9	607	4.02	1.26	4.39	0.418	161	52.9	1.84	15.20	1.68	3.59	5.11	784
4	Y4-2-4	16.56	4.54	2.03	0.88	0.88	69.1	643	2.94	1.62	4.82	0.429	204	44.1	1.5	14.70	1.71	3.87	7.41	1191
5	Y4-2-5	12.01	4.00	1.67	0.74	1.01	88.8	694	7.53	9.99	10.8	0.856	236	105	3.38	47.00	12.20	13.30	27.00	2986
6	Y4-2-6	12.65	5.35	1.38	0.95	0.88	84.2	702	4.13	1.13	6.32	0.546	229	57.7	1.96	21.80	1.69	4.15	5.37	1335
7	Y4-2-7	13.13	4.38	1.66	0.84	0.85	86.5	746	4.46	1.08	6.39	0.544	228	59.3	2.03	16.00	2.13	5.07	5.21	1347
8	Y4-2-8	14.64	4.64	1.75	0.89	0.87	83.7	739	4.23	0.906	5.01	0.432	212	51.9	1.76	14.60	1.62	4.39	4.99	1089
9	Y4-2-9	13.06	4.61	1.57	0.85	0.90	102	827	6.71	1.45	9.68	0.784	256	95.5	3.23	25.50	3.44	6.68	11.00	2190
10	Y4-2-10	16.04	4.59	1.98	0.90	0.93	85.8	762	4.31	0.868	4.74	0.416	230	50.4	1.68	13.70	2.18	3.57	5.38	904
11	Y4-2-11	14.93	4.42	1.92	0.97	0.92	86.2	794	4.59	0.929	5.56	0.478	243	54.4	1.77	14.50	2.23	3.97	5.64	1011
12	Y3-2-1	13.95	4.41	1.70	0.83	0.96	91.4	742	5.41	1.58	6.82	0.588	210	70.2	2.4	14.50	1.52	4.95	5.68	1424
13	Y3-2-2	14.80	4.43	1.80	0.92	0.99	99.8	771	4.59	1.67	5.91	0.514	218	58.1	1.97	12.10	7.78	3.61	4.68	1197
14	Y3-2-3	14.03	4.44	1.74	0.86	0.99	99.6	798	5.07	1.87	5.61	0.473	208	64.7	2.21	15.30	2.71	4.81	6.00	1035
15	Y3-2-4	15.82	4.53	1.89	0.84	0.95	92.4	763	5.33	1.62	6.02	0.55	209	62.4	2.12	18.60	2.30	4.65	6.80	1209
16	Y3-2-5	13.31	4.55	1.68	0.86	0.95	79.9	721	4.56	1.41	6.39	0.549	198	53.6	1.79	17.00	1.66	3.53	4.99	1209
17	Y3-2-6	15.26	4.51	1.88	0.84	0.96	81.6	688	4.84	2.41	5.51	0.487	179	60.2	2.05	13.40	1.92	3.75	6.23	1161
18	Y3-2-7	12.60	4.97	1.44	1.00	0.89	88.7	796	4.99	1.24	6.56	0.546	241	71.6	2.33	24.40	1.88	4.45	7.46	1424
19	Y3-2-8	15.87	5.01	1.79	0.85	0.88	78.2	686	4.3	1.99	5.1	0.44	194	52.2	1.68	11.80	1.81	3.61	4.36	993
20	Y3-2-9	17.13	4.67	2.13	0.81	0.92	75	669	4.35	2	4.09	0.374	175	44	1.48	11.40	2.04	3.24	3.57	790
21	Y3-2-10	15.54	4.95	1.86	0.84	0.89	100	832	5.13	1.91	5.61	0.489	232	60.6	2.01	14.90	2.41	3.88	5.20	1113
22	Y3-2-11	17.11	5.13	1.86	0.86	0.85	90.4	776	4.38	2.29	4.12	0.378	214	49	1.68	9.61	4.06	2.85	2.63	700
23	Y2-2-1	14.16	4.56	1.75	0.85	0.88	66.6	649	4.47	2.68	7.63	0.604	282	64.7	2.14	28.80	3.81	5.86	14.50	2250
24	Y2-2-2	12.61	4.72	1.49	0.82	0.89	89.5	784	6.32	1.63	9.12	0.754	242	76.8	2.71	23.10	2.10	4.73	8.41	2119
25	Y2-2-3	15.80	4.68	1.91	0.86	0.90	79.5	682	3.68	1.22	3.54	0.314	180	42.4	1.42	10.00	1.96	2.88	4.10	640
26	Y2-2-4	12.21	4.66	1.50	0.84	0.92	80.2	678	4.73	3.4	7.87	0.67	215	58.9	1.98	17.10	4.78	4.38	6.60	1813
27	Y2-2-5	11.14	4.40	1.38	0.81	0.91	67.9	462	5.25	1.67	6.11	0.477	190	71	2.13	18.60	1.89	5.33	10.50	1323
28	Y2-2-6	11.56	4.54	1.48	0.89	0.92	92.4	783	5.38	2.52	6.93	0.554	259	65	2.1	16.90	2.33	4.44	6.27	1484
29	Y2-2-7	12.07	4.29	1.61	0.73	0.95	91.6	710	7.61	3.23	8.63	0.651	227	81.2	2.61	38.60	10.30	6.36	25.40	2149
30	Y2-2-8	15.61	4.58	1.94	0.57	1.04	84.3	665	12.8	3.03	11.6	0.847	214	104	3.22	43.50	6.56	7.32	33.80	3280
31	Y2-2-9	13.13	4.54	1.61	0.95	1.13	116	881	5.15	2.1	5.55	0.486	214	55.7	1.95	17.40	5.58	3.68	4.67	1059
32	Y2-2-10	8.67	4.58	1.09	0.84	1.06	64.3	477	4.33	2.18	5.99	0.485	158	49.2	1.67	36.80	7.98	4.08	7.62	1490
33	Y2-2-11	14.49	4.49	1.73	0.91	1.09	110	836	5.44	2.06	6.22	0.524	209	59.2	2.06	18.90	3.68	3.91	5.86	1197
34	Y7-2-1	10.54	4.05	1.56	0.66	1.06	122	755	12.5	5.12	16.2	1.23	254	153	4.82	64.00	5.80	17.40	27.20	4147
35	Y7-2-2	16.67	4.74	2.04	0.85	0.95	83.3	837	4.72	3.17	5.16	1.29	221	54.8	1.82	16.00	22.90	37.10	5.28	844
36	Y7-2-3	13.03	5.03	1.52	0.89	0.95	94.4	910	6.98	4.32	9.76	0.793	262	93.8	3.17	20.20	2.38	21.10	7.72	2178
37	Y7-2-4	13.52	4.90	1.65	0.85	0.93	92.7	347	6.29	4.02	8.32	0.714	260	81.8	2.69	19.60	2.96	17.70	7.08	1771
38	Y7-2-5	17.19	4.55	2.24	0.76	1.02	78.1	761	4.91	3.2	5.26	0.593	190	57.9	1.92	16.80	6.29	9.09	5.98	1053
39	Y7-2-6	15.39	4.75	1.89	0.83	0.96	72.9	669	4.53	2.64	4.83	0.516	193	55.7	1.87	16.90	5.26	7.09	5.54	1113
40	Y7-2-7	10.92	3.95	1.72	0.64	0.95	78.5	664	7.18	61.7	8.64	0.732	297	88.7	2.88	63.90	18.00	31.20	15.30	2059
41	Y7-2-8	11.90	4.32	1.64	0.72	0.95	94	754	8.8	2.24	9.78	0.8	246	101	3.24	63.50	7.41	12.60	37.30	2956
42	Y7-2-9	12.02	4.34	1.67	0.70	1.00	90.2	777	9.57	1.76	10	0.761	254	113	3.73	55.90	6.18	9.35	35.70	3142
43	Y7-2-10	8.89	4.00	1.30	0.65	1.04	123	725	11.1	17.3	13.5	1.02	234	129	3.95	102.00	23.70	22.00	51.90	3734
44	Y7-2-11	7.58	2.95	1.58	0.63	1.08	112	778	12.3	10.9	13.1	0.964	268	130	4.31	64.60	31.00	20.30	46.10	3717

Table 1. Cont.

No.	SampleNo.	P	Ni	Sr/Ba	V/(V + Ni)	V/Cr	Ni/Co	Sr/cu	Zr/Sc	Th/Sc	La/Sc	Ti/Zr	La/Th
1	Y4-2-1	126	3.95	0.31	0.86	2.72	1.31	38.39	25.50	1.92	5.53	19.07	2.88
2	Y4-2-2	119	2.00	0.30	0.90	2.18	1.61	47.37	27.23	2.03	6.43	16.99	3.16
3	Y4-2-3	119	2.04	0.27	0.88	2.97	1.21	44.85	36.74	2.79	10.97	14.82	3.93
4	Y4-2-4	172	2.32	0.32	0.86	1.98	1.36	52.71	26.41	1.76	12.10	27.01	6.87
5	Y4-2-5	344	16.90	0.34	0.74	1.74	1.39	17.74	15.11	1.08	4.89	28.44	4.52
6	Y4-2-6	146	2.29	0.33	0.90	4.06	1.36	55.18	28.99	2.08	8.04	23.13	3.87
7	Y4-2-7	325	2.69	0.31	0.86	3.07	1.26	44.97	29.80	2.24	9.05	22.71	4.04
8	Y4-2-8	199	2.05	0.29	0.88	2.93	1.27	48.29	31.45	2.56	10.73	20.99	4.18
9	Y4-2-9	185	3.80	0.31	0.87	2.32	1.10	38.32	26.98	1.90	6.89	22.94	3.64
10	Y4-2-10	106	2.49	0.30	0.85	2.55	1.14	64.43	26.67	2.28	10.21	17.93	4.48
11	Y4-2-11	93	2.45	0.31	0.86	2.57	1.10	61.21	28.63	2.42	9.89	18.59	4.10
12	Y3-2-1	99	2.03	0.28	0.88	2.55	1.34	42.42	34.08	2.63	10.19	20.29	3.88
13	Y3-2-2	106	3.80	0.28	0.76	2.59	0.49	60.39	33.58	2.65	11.33	20.60	4.27
14	Y3-2-3	139	2.49	0.26	0.86	2.55	0.92	43.24	30.52	2.39	10.33	16.00	4.32
15	Y3-2-4	113	2.79	0.27	0.87	2.74	1.21	44.95	25.89	2.21	9.79	19.37	4.43
16	Y3-2-5	132	1.73	0.27	0.91	3.41	1.04	56.09	30.45	2.59	10.97	22.55	4.23
17	Y3-2-6	146	1.96	0.26	0.87	2.15	1.02	47.73	35.41	2.85	12.76	19.29	4.48
18	Y3-2-7	199	2.23	0.30	0.92	3.27	1.19	54.16	28.08	1.96	6.27	19.89	3.21
19	Y3-2-8	152	1.91	0.28	0.86	2.71	1.06	53.74	36.25	2.99	13.61	19.03	4.56
20	Y3-2-9	126	1.86	0.26	0.86	3.19	0.91	54.01	32.84	3.25	15.07	17.95	4.64
21	Y3-2-10	132	2.05	0.28	0.88	2.87	0.85	59.79	28.72	2.43	9.72	18.37	4.00
22	Y3-2-11	113	2.01	0.28	0.83	3.65	0.50	75.09	39.52	3.53	15.08	14.29	4.27
23	Y2-2-1	258	4.66	0.43	0.86	1.99	1.22	48.12	19.09	1.32	6.81	34.78	5.17
24	Y2-2-2	159	2.76	0.31	0.89	2.75	1.31	51.16	28.03	2.31	7.70	27.59	3.34
25	Y2-2-3	119	1.75	0.26	0.85	2.44	0.89	62.50	32.37	2.81	13.97	15.10	4.97
26	Y2-2-4	146	3.78	0.32	0.82	2.59	0.79	49.09	29.90	2.40	9.59	30.79	4.00
27	Y2-2-5	172	2.50	0.41	0.88	1.77	1.32	35.65	24.57	1.82	6.51	18.63	3.58
28	Y2-2-6	132	2.21	0.33	0.88	2.70	0.95	58.33	28.26	2.34	7.57	22.83	3.23
29	Y2-2-7	457	14.70	0.32	0.72	1.52	1.43	35.69	15.65	1.47	5.84	26.46	3.98
30	Y2-2-8	464	9.86	0.32	0.82	1.29	1.50	29.23	19.29	2.37	8.00	31.53	3.37
31	Y2-2-9	106	2.61	0.24	0.87	3.73	0.47	58.15	30.44	2.81	10.60	19.02	3.77
32	Y2-2-10	960	3.30	0.33	0.92	4.83	0.41	38.73	18.43	1.62	6.07	30.29	3.74
33	Y2-2-11	119	2.61	0.25	0.88	3.23	0.71	53.45	28.06	2.58	9.76	20.22	3.79
34	Y7-2-1	848	10.10	0.34	0.86	2.35	1.74	14.60	18.21	1.49	5.04	27.11	3.38
35	Y7-2-2	139	5.32	0.26	0.75	3.03	0.23	5.96	35.13	3.03	15.64	15.40	5.17
36	Y7-2-3	185	2.21	0.29	0.90	2.62	0.93	12.42	37.22	2.77	10.24	23.22	3.70
37	Y7-2-4	179	2.55	0.75	0.88	2.77	0.86	14.69	31.83	2.45	9.61	21.66	3.93
38	Y7-2-5	166	3.11	0.25	0.84	2.81	0.49	20.90	28.38	2.41	13.04	18.19	5.42
39	Y7-2-6	139	2.66	0.29	0.86	3.05	0.51	27.22	27.57	2.24	10.94	19.98	4.88
40	Y7-2-7	2543	16.90	0.45	0.79	4.18	0.94	9.52	16.61	1.34	11.78	23.21	8.76
41	Y7-2-8	192	11.10	0.33	0.85	1.70	1.50	19.52	14.33	1.25	4.07	29.27	3.26
42	Y7-2-9	192	9.38	0.33	0.86	1.57	1.52	27.17	18.37	1.56	4.96	27.81	3.19
43	Y7-2-10	364	23.60	0.32	0.81	1.97	1.00	10.64	10.32	0.89	2.73	28.95	3.07
44	Y7-2-11	1424	25.60	0.34	0.72	1.40	0.83	13.20	12.62	1.19	3.85	28.59	3.23

5. Discussion

5.1. Sedimentary Sorting and Recycling

Detailed geological data obtained in recent years have shown that LREEs (Th, Sc, La and Zr) are chemically stable and not easily fractionated during the deposition cycle. Moreover, these elements are insoluble in water and are thus negligibly affected by metamorphism [39,40]. LREEs can be used as primary indicators to distinguish rock types in provenance areas. Therefore, Th/Sc and Zr/Sc ratios can be used to constrain the parent rock components. The Th/Sc ratios measured in the sandstone samples from the study area varied between 0.89 and 3.03, with an average of 2.20, exceeding the upper crustal Th/Sc ratio of 1.0. The Zr/Sc ratio for the samples ranged from 10.32 to 39.52 and showed a significant positive correlation with the Th/Sc ratios (Figure 7). Moreover, the relationship between the two ratios formed an unparallel trend line to the depositional cycle, implying compositional homogeneity and minimal influence of sedimentary sorting. To summarize, it can be concluded that the fine-grained sandstones of Sifangtai Group are first-cycled sediments and undergo no or minimal mineral sorting.

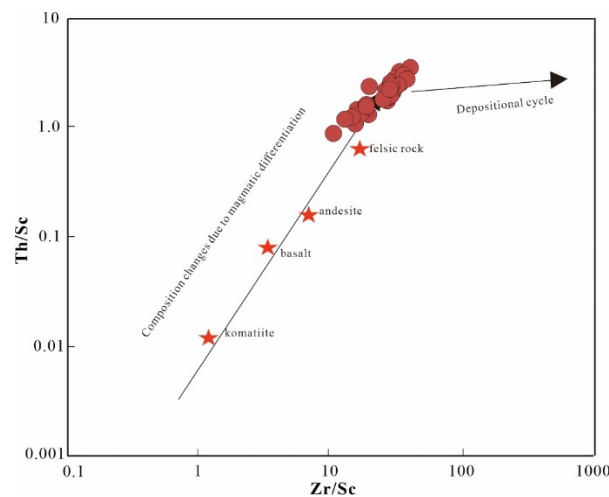


Figure 7. Th/Sc-Zr/Sc diagram of sandstone of the Sifangtai Formation in northwest Songliao Basin (after McLennan et al. [22]).

5.2. Weathering Degree

The degree of provenance chemical weathering is dominated by the source rock composition, duration of weathering, climatic conditions, and tectonic activities [20,41–44]. Ca, Na, and K are typically removed during the weathering of source rocks, and the residual amounts of these elements in soil profiles and sediments are sensitive indicators for determining the degree of chemical weathering. The chemical index of alteration (CIA) is considered an effective indicator of the degree of source weathering, where CIA values from 50–60 and 60–80 suggest weak weathering and moderate weathering, respectively [42–44]. Moreover, the index chemical variation (ICV) can be used to determine the compositional maturity of the sediment; high ICV values represent low sedimentary component maturity and strong tectonics, while low ICV values represent high maturity of sedimentary components and relatively stable tectonics. The plagioclase index of alteration (PIA) can also be used to assess the source weathering and elemental redistribution during diagenesis [42–44].

The CIA values of the sandstone samples from the Sifangtai Formation ranged from 51.99–62.07, with an average of 54.35, indicating that the parent rocks were subjected to weak weathering. The ICV values of the samples ranged from 0.60 to 1.03, with an average of 0.69, suggesting immature parent rocks (Figure 8a). Moreover, all the sandstone samples showed an evolutionary trend of weak weathering when plotted in a CIA-ICV plot, which revealed a dominant granite parent rock for the samples (Figure 8b).

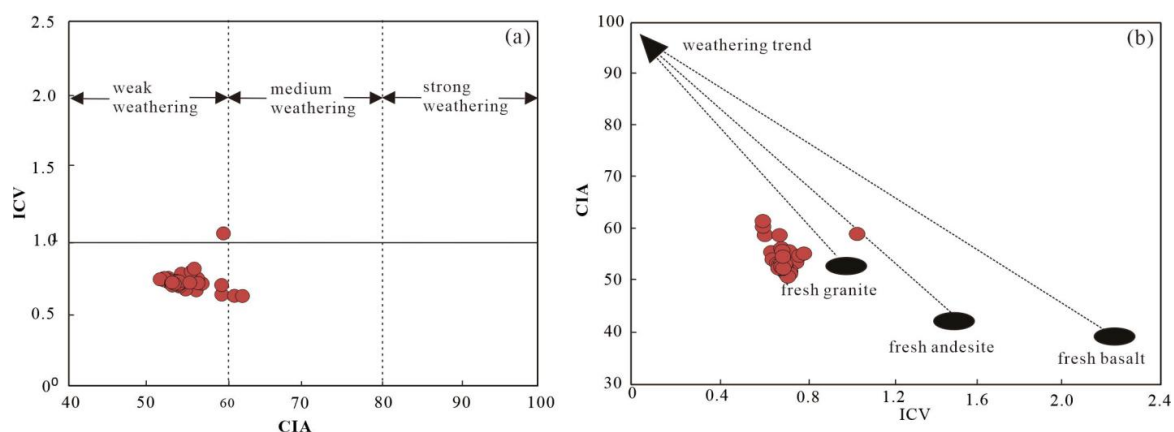


Figure 8. Sandstones of the Sifangtai Formation in the northwest of Songliao Basin, (a) CIA-ICV diagram, (b) ICV-CIA diagrams (modified after Cox et al. [40]).

Besides the CIA, the PIA can also determine the weathering intensity of plagioclase. Unweathered rocks have PIA values around 50, and weathered clay mineral PIA values in weathered clay minerals are close to 100 [45,46]. Sifangtai Formation sandstone PIA = 54.01–66.33. It reflects the weak chemical weathering of the sandstone source area of the Sifangtai Formation.

5.3. Depositional Environment

5.3.1. Paleosalinity Determination

The Sr and Ba content of rocks and their ratios can be used to determine the placement of the medium. An Sr content range of 200–300 ppm in sandstones represents a freshwater depositional environment, whereas 200–1000 ppm indicates a marine environment [47]. Moreover, Sr/Ba ratios can also be used to constrain the depositional environment of formation, with ratios > 1 indicating a marine environment and ratios < 1 suggesting a freshwater environment. In this study, Sr concentration of the samples ranged from 161 to 297 ppm, and Sr/Ba ratios ranged between 0.25 and 0.75, indicating that uranium-bearing sandstones in the study area were deposited in a freshwater environment (Figure 9).

5.3.2. Palaeoredox Conditions

The elements V, Ni, Cr and Co are characterized by the following unique characteristics: they do not readily migrate during diagenesis, they are autogenously enriched in oxygen-poor depositional environments, they are readily soluble under oxidizing conditions, and they maintain a pristine sedimentary record. Therefore, the content of these elements in rocks can be used to constrain depositional oxidation-reduction environments.

Jones et al. [48] reported that V/Cr, Ni/Co, and V/(V + Ni) ratios are the most reliable parameters for determining the oxidation-reduction environment of hydrological bodies during sediment deposition by studying the paleooxic phases of Late Jurassic dark mudstones and sandstones in Northwest Europe.

The ratio of V/(V + Ni) is typically used to determine the degree of water stratification during sediment deposition, where ratios between 0.4 and 0.6 indicate weak stratification and oxygen-poor depositional environments, ratios between 0.6 and 0.8 suggest medium stratification and a sub-oxygenated environment, and ratios > 0.8 represent strong stratification and an oxygen-rich environment. In this study, the ratios of the samples ranged from 0.72 to 0.92, with an average ratio of 0.85, suggesting that the hydrological depositional environment was rich in oxygen and characterized by significant stratification (Figure 9).

V and Cr display relatively similar characteristics; both are readily enriched in sediments in reducing environments and are water-soluble in oxidizing environments. As shown in Figure 9, we obtained relatively consistent results in our analysis of the redox

state by applying these indexes. Overall, our analyses suggested an oxygen-rich water environment.

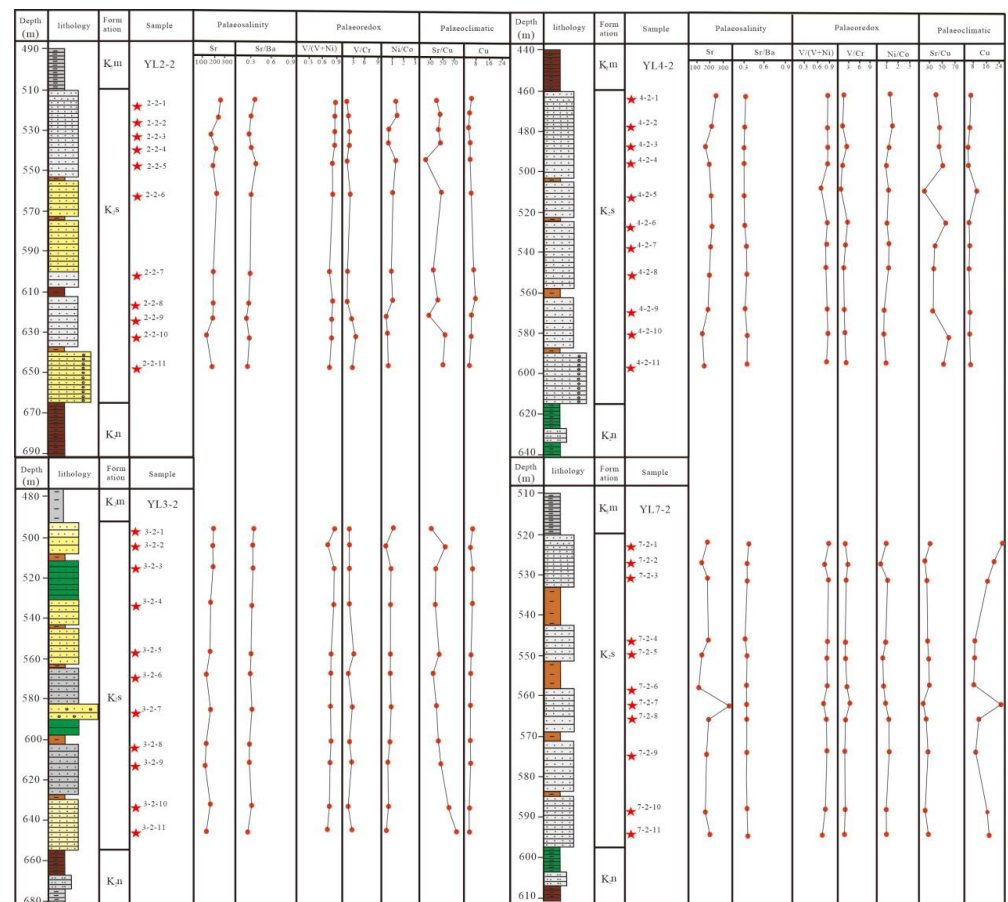


Figure 9. Discrimination diagram of the ratio of trace elements in the Sifangtai Formation sandstone in the study area.

5.3.3. Paleoclimate Conditions

Elemental geochemical signatures can be used to effectively reconstruct paleoclimatic conditions. For example, Sr and Cu content as well as Sr/Cu ratios are suitable parameters for reconstructing the paleoclimate. Previous studies have also shown that a Sr/Cu ratio between 1.3 and 5 indicates a wet climate, whereas ratios > 5 denote arid climates [49,50]. In this study, the Sr/Cu ratios of the samples were > 5, implying arid climatic conditions during sandstone deposition (Figure 9).

In addition to the Sr/Cu ratio, SiO₂/Al₂O₃ reflects the extent of chemical leaching and dissolution transport in host rocks. SiO₂/Al₂O₃ ratios < 4 denote wet environments and long transportation distances, and ratios > 4 indicate arid environments and short transportation distances [6,7]. In this study, we obtained SiO₂/Al₂O₃ ratios of the sandstone samples between 4.54 and 9.46, indicating arid climatic conditions.

5.4. Provenance Conditions

Our elemental geochemical analysis of the sandstone samples from the Sifangtai Formation indicated that the sandstone was predominately derived from the upper crust. Table 1 shows that TiO₂ concentration varied between 0.11 wt% and 0.69 wt%, with an average value of 0.28%; Al₂O₃ content ranged from 8.71 wt% to 15.06 wt%, with an average of 11.15%; Ni content ranged from 1.73 ppm to 23.60 ppm, with an average of 5.25 ppm; and Zr content ranged from 44.00 ppm to 130 ppm, with an average of 71.61 ppm. On a graph of TiO₂ versus Al₂O₃, all the samples were plotted in the area between calc-alkaline

granite and granodiorite (Figure 10a [51]). As illustrated by the TiO_2 -Zr, K_2O -Rb and TiO_2 -Ni diagrams, all the samples were clustered in the acid volcanic rock region of the plots (Figure 10b–d [52–54]). Therefore, these results suggest a felsic source area for the Sifangtai Formation sandstones.

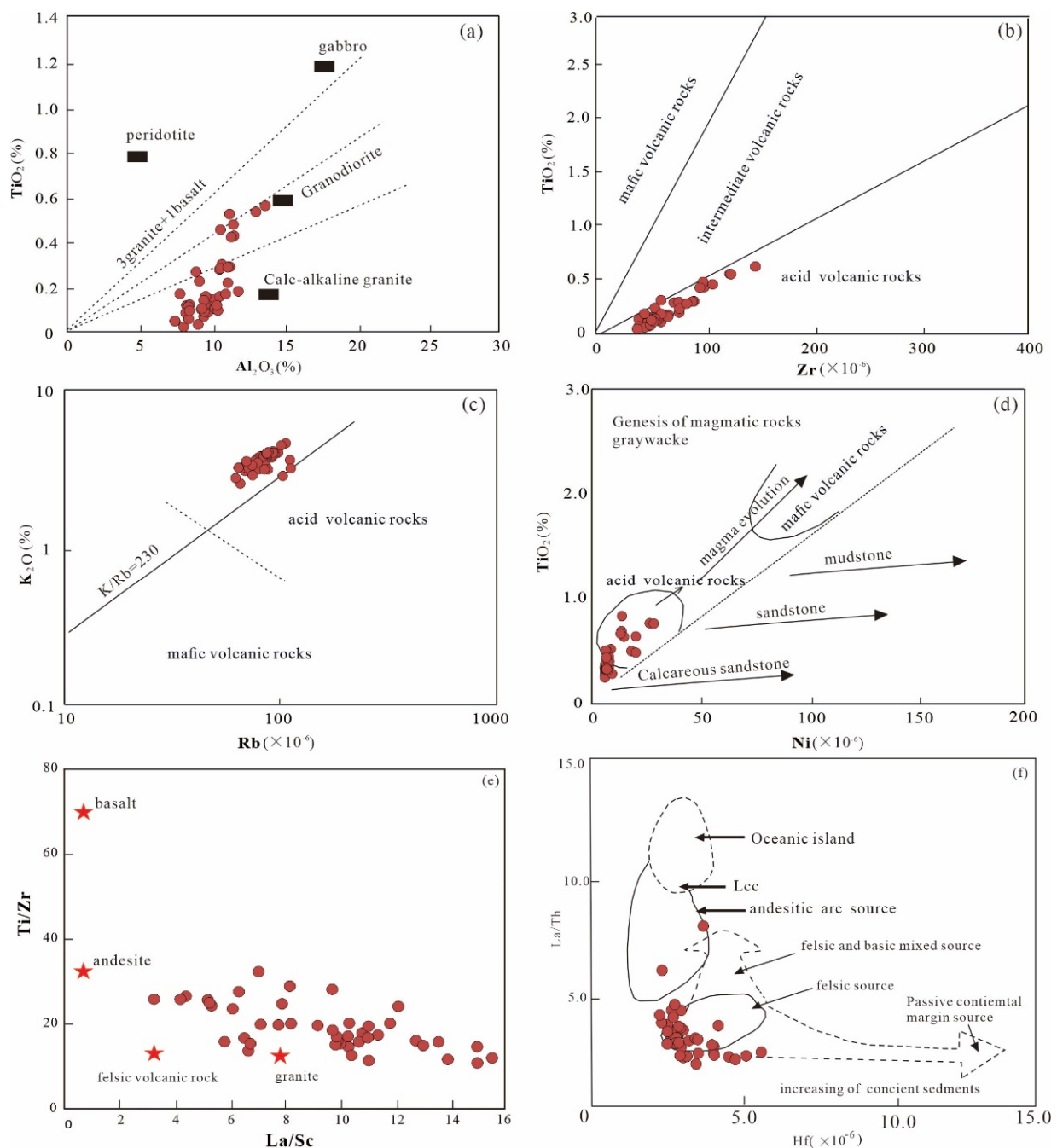


Figure 10. Discriminant diagram of source rock properties of major and trace elements in Sifang Formations in the northern Songliao Basin. (a) TiO_2 - Al_2O_3 (after Schieber [51]), (b) TiO_2 -Zr (after Hayashi et al. [52]); (c) Rb- K_2O (after Floyd and Leveridge [53]); (d) Ni- TiO_2 (after Floyd [54]); (e) Ti/Zr - La/Sc and (f) La/Th - Hf (after Bhatia and Crook [55]).

To analyze the source rock properties of clastic rocks in the study area, Ti/Zr - La/Sc and La/Th - Hf trace diagrams were used for a direct analysis. The Ti/Zr ratios of the sandstone samples varied significantly from 14.29 to 34.78, with an average ratio of 22.29. The La/Sc ratio also showed a similar trend of significant variation ($\text{La}/\text{Sc} = 2.73$ – 15.08 , average = 9.19). Moreover, the sandstone samples were plotted between felsic volcanic

rocks and granites in the Ti/Zr-La/Sc diagram (Figure 10e [55]) and almost exclusively in the felsic volcanic rock region on the La/Th-Hf diagram (Figure 10f [55]). These results further confirmed an intermediate felsic source for the Sifangtai Formation sandstones.

In the present study, the patterns and characteristics of REEs in the sandstone samples were used to confirm the parent material of the uranium-bearing sandstone unit in the study area. Previous studies have demonstrated that felsic rocks typically exhibit high LREE/HREE ratios and negative Eu anomalies. Conversely, mafic rocks display low LREE/HREE ratios and almost no significant Eu anomalies. In our samples, the REE distribution pattern was right-inclined (Figure 6a), showing relatively enriched LREE and depleted HREE characteristics and weak Eu negative anomalies ($\delta\text{Eu} = 0.57\text{--}1.00$). Therefore, these results further confirmed an intermediate felsic parent rock for the uranium-bearing sandstone unit in the study area.

To determine the specific intermediate felsic parent rock of uranium-bearing sandstone in the study area, the geochemical characteristics of the felsic rocks in the Xiaoxing'an and Zhangguangcailing areas around the Songliao Basin were analyzed (Figure 11) [56–62]. The geochemical characteristics of these units were highly consistent with the REE partitioning pattern of the Sifangtai Formation sandstones in the study area. Combined with the location of the study area, we deduced that the Sifangtai Formation sediments in the northern region of the Songliao Basin most likely served as the source region for sediments in the Xiaoxing'an and Zhangguangcailing areas.

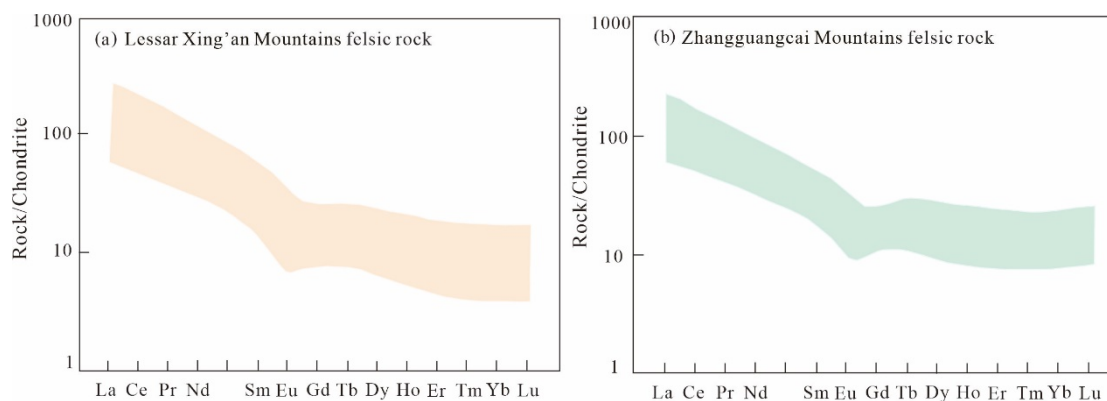


Figure 11. Distribution of rare earth elements in felsic rocks in the Xiaoxing'anling and Zhangguangcailing areas (after [7,56–62]). (a) Lessar Xing'an Mountains felsic rock, (b) Zhangguangcai Mountains felsic rock.

The study area is predominately located in the northern plunge and central downwarp of the Songliao Basin. Therefore, the Zhang Guangcai Ridge in the east, the Xiao Xing'an Ridge in the northeast, and the Daxing'an Ridge and surrounding areas in the west are all potential source areas for the Sifangtai Formation. During the Late Cretaceous, the Songliao Basin was controlled by the transformation of the Paleo-Asian tectonic system into the Paleopacific tectonic domain system. The basin experiences northwestward stress compression, whereas the southeast is relatively uplifted, and sedimentation and subsidence occurring in the center of the basin continue to shift in a northwestern direction [63,64]. Therefore, the possibility of the Daxing'an Ridge serving as the sediment source for the Sifangtai Formation is highly unlikely.

Furthermore, during the Early Cretaceous, magmatism was prominent in the Daxing'an Ridge (particularly between 110 and 150 Ma). Moreover, numerous studies have demonstrated a general lack of clastic rocks with ages between 110 Ma and 150 Ma in this area [65–67]. Therefore, based on the sedimentary-tectonic evolution and isotope dating results, we concluded that the Daxing'an Ridge does not serve as the source area for the Sifangtai Formation.

Based on the results of the age dating analysis of three detrital zircons obtained from the Sifangtai Formation sandstone, the following ages were obtained: 80–105 Ma,

175–240 Ma, and 1.8 Ga [68]. The zircon age of 1.8 Ga has been reported in boreholes within and around the basin. It is still mainly concentrated in the northern region of the Songliao Basin. The Sifangtai Formation was formed from a sequence of layers deposited from the late tectonic movements of the Nengjiang Formation, during which the southeastern region of the basin underwent denudation. Therefore, the 1.8 Ga zircon age indicates sources from the northern region of the basin. The 80–105 Ma age range corresponds with Late Cretaceous magmatism, which was widespread in eastern Jihei, and the 175–240 Ma age range corresponds with the Late Triassic–Middle Jurassic age of the Zhangguangcai Ridge in eastern Songliao [68]. In summary, the peak detrital zircon ages coincide with ages obtained for the Zhang Guangcai Ridge, eastern Jihei, and northern basin areas. Moreover, the sand body shows significant spreading characteristics in a north–south direction, and the depositional environment transitioned from a partial oxidation environment in the north to a partial reduction environment in the south, with a gradual weakening in the hydrodynamic force. Accordingly, the Xiaoxing’an Ridge served as the predominant sediment source for the Sifangtai Formation, followed by the eastern region of Jihei and Zhangguangcailing.

In addition, the distribution map of water systems in the northern part of the Songliao Basin has shown that six major water systems are developed in the basin, among which the Nehe and Baiquan water systems are the main ones in the study area (Figure 12), which can provide a constant source of material for the sandstones of the Sifangtai Formation. The distribution of this water system is also mainly located in the tectonic position of the Xiaoxing’an and Zhangguangcailing areas.

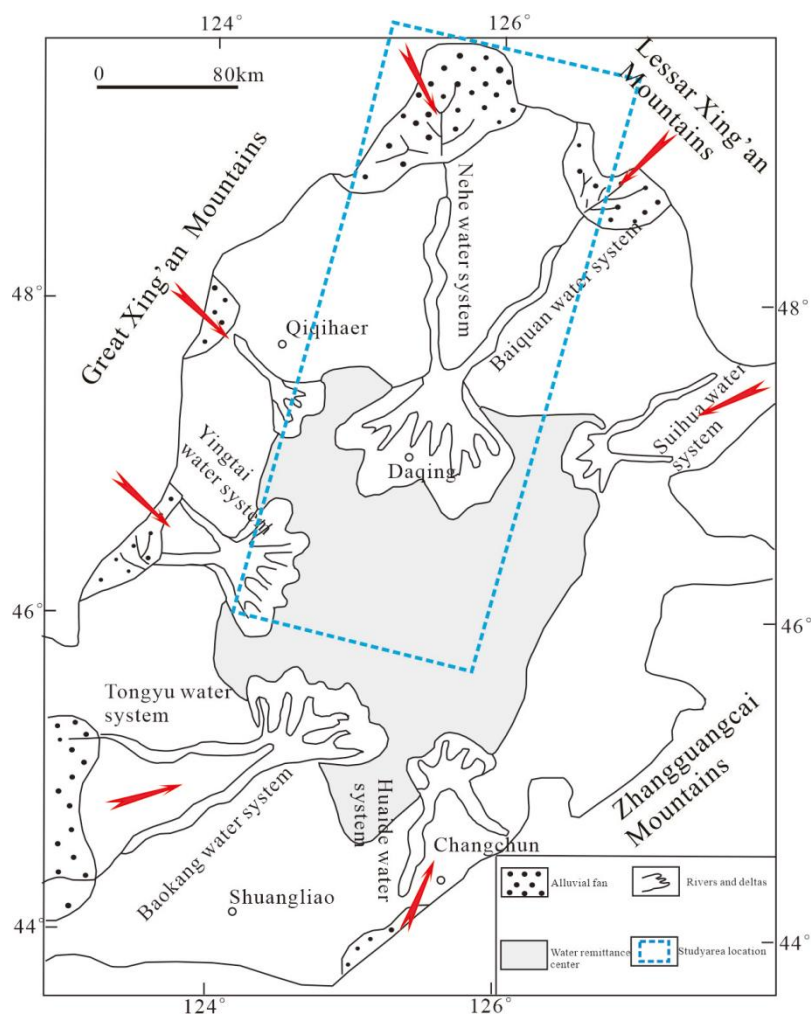


Figure 12. Distribution of water systems in the Songliao Basin.

5.5. Tectonic Background

The siliciclastic rocks in the study area were derived from different tectonic settings and display terrain-specific characteristics [51–55]. Numerous tectonic discrimination diagrams for sedimentary basins have been proposed based on major and trace element compositions [69–71]. As illustrated in Figure 13, the sandstone samples clustered in the diagram in the active continental margin region, and the tectonic setting was relatively similar, reflecting a strong subduction plate regime.

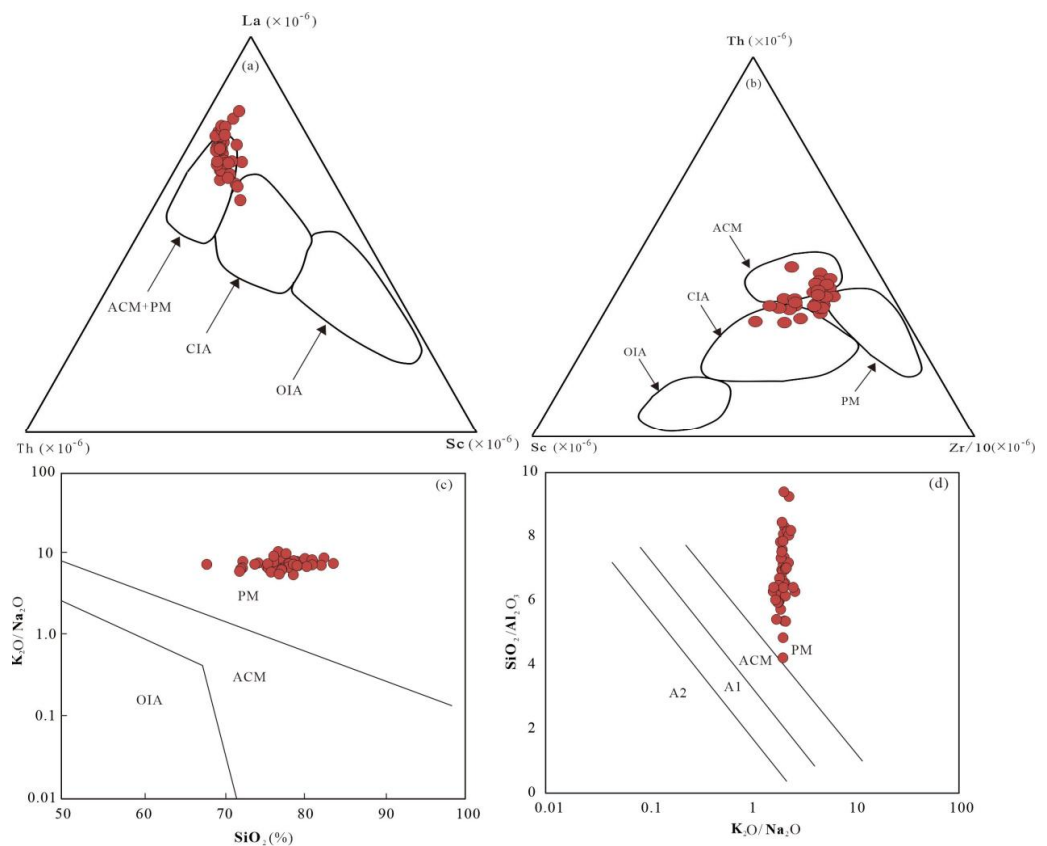


Figure 13. Discriminant map of provenance of sandstone Sifangtai Formation in the northern Songliao Basin: (a) La-Th-Sc and (b) Th-Sc-Zr/10 (after Xia et al. [6]) (c) K_2O/Na_2O - SiO_2 (after Roser and Korsch. [69]); (d) SiO_2/Al_2O_3 - K_2O/Na_2O (after Maynard et al. [70]).

Furthermore, REEs are often used to determine the tectonic properties of clastic rocks. McLennan [21] used PAAS for standardization and found different values of δCe in different tectonic contexts, where a significantly negative δCe anomaly denoted a spreading oceanic ridge, a moderate negative δCe anomaly indicated an ocean basin, and a weak negative δCe anomaly indicated a continental margin zone. The δCe of the sandstone samples obtained from the Sifangtai Formation ranged from 0.85 to 1.13, with an average of 0.95, suggesting that the depositional environment of this formation was an active continental margin environment.

This finding was further supported by the following geological observations of the study area: In terms of tectonic position, the northern region of the Songliao Basin crosses the Xingmeng Orogenic Belt and represents the superposition of the Pacific tectonic and the ancient Asian Oceanic tectonic system. Since the Mesozoic, it has undergone significant tectonic deformation and orogenesis, and the rocks comprising the basin were formed in a subducting plate tectonic setting, whereby the Pacific Ocean Plate subducted in a southward direction [72,73].

In addition, the Songliao Basin is a faulted Meso-Cenozoic basin, and previous studies have reported a wide distribution of felsic rocks in the Xiaoxing'anling and Zhangguang-

cailing areas, including the fine-grained synogranite of the Dong'an Gold Mine in the Xiaoxing'an Mountains, which were formed 184 Ma in an ancient active continental margin setting of the subducting Pacific Plate [74]. Moreover, based on the study conducted by Ge et al. [75], combined with previously published geochronological and geochemical data, we inferred that the Xiao Hinggan-Zhangguangcai Mountains formed in an active continental margin setting during the Late Paleozoic to Mesozoic. Finally, the Early Jurassic granite of the southern Zhangguangcai Mountains formed in a post-collisional tectonic setting, representing an extensional episode in the collisional event, and the geotectonic setting was an extensional tectonic setting after subduction of the Pacific Plate [76].

Overall, our results indicate that the host rocks of the Sifangtai Formation are predominantly felsic, and this observation is consistent with rocks in the northern Xiaoxing'an Ridge and Zhangguangcailing regions. Combining previous research results and the elemental geochemical characteristics of the sandstone samples obtained in the present study, we concluded that the sandstones of the Sifangtai Formation formed in an active continental margin environment closely related to Pacific subduction.

5.6. Relationship between the Sandstones and Uranium Mineralization

For sandstone uranium ores, the mineralization potential is generally analyzed in terms of the uranium source conditions, tectonic evolution, sand bodies, post-generation alteration (oxide zone development), paleoclimatic conditions, and known uranium mineralization anomalies [1–6].

5.6.1. Uranium Source Conditions

As mentioned, the source area of the Sifangtai Formation sandstone was determined as an active continental margin tectonic environment, and the parent rocks were felsic and sourced from the Xiaoxing'an and Zhangguangcailing areas. The average uranium content of granite from these areas ranged from 7.02 to 5.93 ppm, and the uranium leaching rate of the granites (percentage of U by weight leached from granite since its formation) was 22.13 wt%, representing a fast leaching rate. The total amount of activated uranium migrating into the basin from the eroded source area in the northern region of the Songliao Basin was 4.32 million tons, indicating that the northern region of the basin is enriched with uranium sources ([28] Table 2). Table 3 shows the average mineral contents of granites from the Zhang Guangcailing-Xiaoxing'an region. Compared with the mineral content of sandstones from the Sifangtai Formation in the study area, these data indicate that the mineral content of orthogranite and diorite is more similar to that of the Sifangtai Formation sandstone. The material source of the sandstone was most likely Triassic-Jurassic orthogranite and diorite granite [74–76].

Table 2. Calculation of the total amount of activated uranium remitted to the basin from uranium-bearing granite alteration source areas in the northern part of the Songliao Basin (after [28]).

Location	Daxing'an Ridge	Xiaoxing'an Ridge	Zhangguangcai Ridge	Total
Erosion source area Space (km ²)	19,000	9800	14,500	
Granite as a percentage of the erosion source area	55%	65%	80%	
Granite exfoliation thickness (m)	100	100	100	
Average uranium content of granite (ppm)	7.4	7.02	5.93	
Granite uranium leaching rate (%)	23.42	22.13	22.13	
Total activated Uranium (10 ⁴ t)	181	99	152	432

Table 3. Average mineral and organic matter content of Sifangtai Formation sandstones and Zhang Guangcailing-Xiaoxinganling granites.

SampleNo.	Lithology	Q (%)	Pl (%)	Kfs (%)	Bi (%)	Lv (%)	TOC (%)	S (%)	C1 μ L/kg
1	Black sandstone	40–45	15–20	15–20	1–3	15–20	0.14	0.08	9183
2	Oxidized Sandstone	35–40	10–15	15–20	1–3	20–25	0.09	0.03	216
3	Syenogranite	35–40	10–15	40–45	1–3	-	-	-	-
4	Monzonitic granite	25–30	25–30	30–35	3–5	-	-	-	-
5	granodiorite	25–30	50–55	5–10	5–10	-	-	-	-

5.6.2. Tectonic Conditions and Uranium Mineralization

The basement faults in the northern region of the Songliao Basin can be categorized into NE- and NW-trending faults, which control the overall evolution of the basin. Uranium mineralization was concentrated at the intersection of the two fracture sets. Overall, six uranium enrichment zones could be identified (Figure 14). Moreover, three primary areas of tectonic influence were determined for the study area: First, deep basement fractures are also located in this area, the base of the Cretaceous formations are developed, and there are also features of tectonic uranium mineralization and anomalous sedimentary layer development [28]. Second, the northern region of the Songliao Basin contains hydrocarbon deposits of the Shahezi and Yingcheng Formations, as well as several oil-gas fields, such as the Jiaoqiao, Erzhan, Pingyang, and Alaxin fields. Tectonic action widening of the ascent pathway for deep reducing (hydrocarbon) fluids. The fracture crosses the Upper Cretaceous and becomes a channel for the upward transport of deep reducing fluids, such as those containing oil-gas and CO₂, forming oil-gas reservoirs, generating extensive reduction alteration in the Sifangtai Formation, and increasing the reduction capacity of the Sifangtai Formation. The sandstones of the Sifangtai Formation in the vicinity of the oil-gas field exhibit low organic carbon and sulfur content and high acidolytic hydrocarbon content, further indicating that oil and gas are the main reducing substances. Uranium mineralization is predominately developed in sandstones near the oil-gas fields, and the ore types are mainly medium- and fine-grained sandstones, with the primary uranium minerals being bituminous uranium ore and uraninite [28]. Finally, tectonic conditions may alter the local groundwater dynamics system for infiltration or discharge zones, complementing and improving the replenishment-runoff-discharge system and promoting the development of interstratified oxidation zones and uranium mineralization [28].

In conclusion, the tectonics of the Sifangtai Formation may promote an improved stratigraphic structure of this formation, with large sand thicknesses and sufficient reduction conditions. Moreover, late-stage tectonic uplift denudation resulted in late-stage modification of the target layer, allowing it to more readily form oxidation zones [77,78].

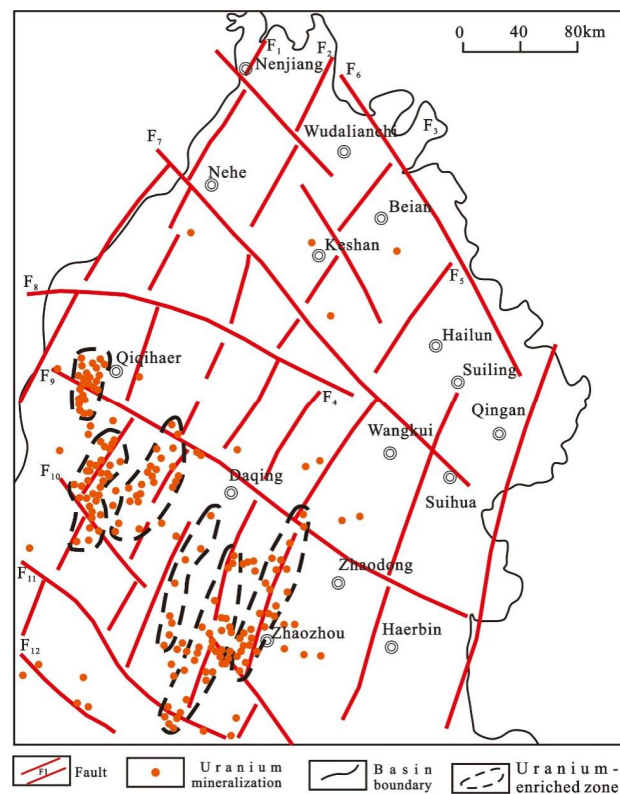


Figure 14. Relationship between basement fractures and uranium mineralization in the northern part of the Songliao Basin (based on [66], slightly modified).

5.6.3. Sand Body Development Conditions

The sand body of the Sifangtai Formation is also markedly developed in the study area, with a relatively shallow burial depth, and it consists of braided river sediment (consistent with the previous elemental geochemical characteristics determined for the sandstone samples). Moreover, the sandstone material has the trend of gradually increasing, and the sand body is characterized by significant thickness and wide spreading. The cumulative thickness of the sand body is 80–100 m (Figure 3c).

The sand body is characterized by loose rocks, and the gap-filling material is mainly clay-powdered, with an approximate content of 1%. Sandstone of the Sifangtai Formation in the vicinity of the oil-gas field is visible as flakes and lamellar charred plant debris, with a large amount of pyrite absorbed on the surface.

5.6.4. Oxidation Zone Development Conditions

An oxidation zone exists in the Sifangtai Formation, and it is developed in the sand body formed by braided river deposition. The oxidation zone can be divided vertically into fully, medium, and weak oxidation zones. The fully oxidized zone in the sand body is yellow in color and does not contain evident carbon residue. Moreover, the sand body in this oxidation zone is loose, and the GR curve reflects a low uranium content. In the medium oxidized zone, the sand body is mainly grayish yellow and light yellow in color, with a thin layer of lenticular sand body and a small amount of charcoal debris. The GR curve for this zone indicates a slight increase in uranium content. The weakly oxidized zone is characterized by a gray and yellow interlayered sand body with visible organic matter (Figure 15). The thickness of the oxidized sand body exceeds 50 m and extends over 50 km, with high oxidation intensity.

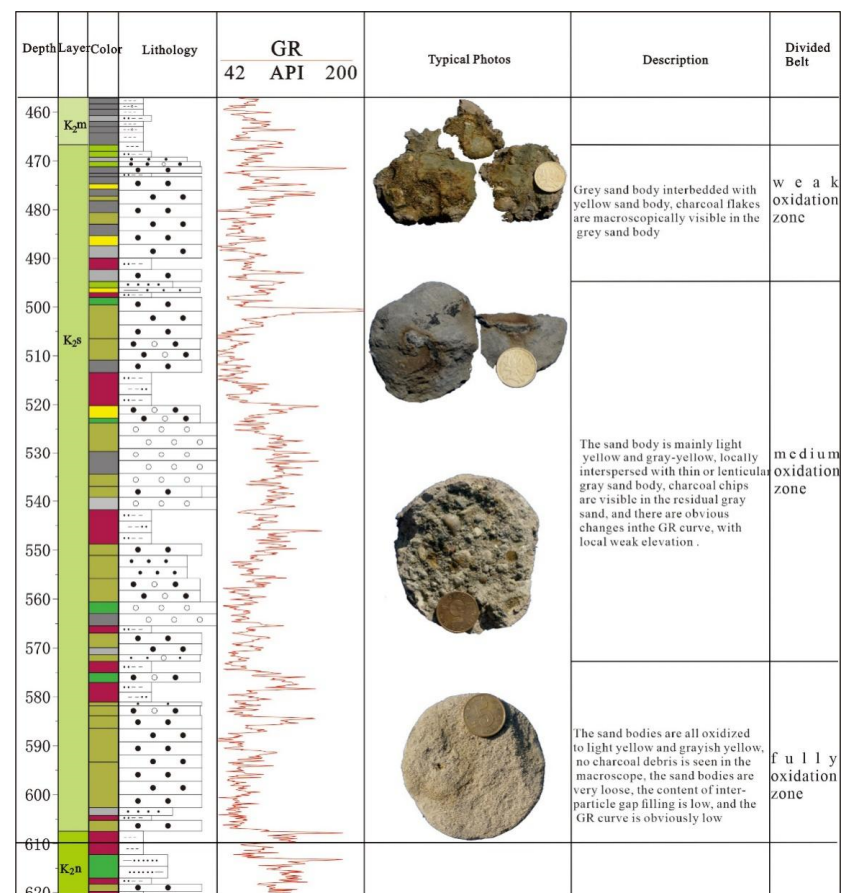


Figure 15. Development characteristics of oxidation zone in Sifangtai Formation of northern Songliao Basin.

5.6.5. Paleoclimatic Conditions

The geochemical characteristics of the major elements indicate that the sandstones of the Sifangtai Formation were formed under semi-arid climatic conditions, and the Late Cretaceous Sifangtai Formation typically comprises gray medium-fine sandstones interspersed with purple-red mudstones, with visible calcareous nodules.

The arid paleoclimatic environment provided the optimal conditions for the formation of uranium-oxygenated water and the pre-enrichment and transport of uranium elements.

5.6.6. Uranium Mineralization Development

Recent exploration in the study area has indicated that uranium mineralization is more developed in the Sifangtai Formation in the northern region of the Songliao Basin.

The uranium mineralization extends steadily over 3 km (Figure 16), and the mineralized lithologies are mainly gray medium sandstone and fine sandstone, which are produced in the sandstone at the bottom of Sifangtai Formation.

In terms of composition, organic carbon and sulfur content is low, while the acidolytic hydrocarbon content is high, indicating that oil and gas are the main reducing substances. The oxidized sandstone is mainly light yellow in color and remains in the gray sandstone in the form of dipping, agglomerates, and stripes (Table 3).

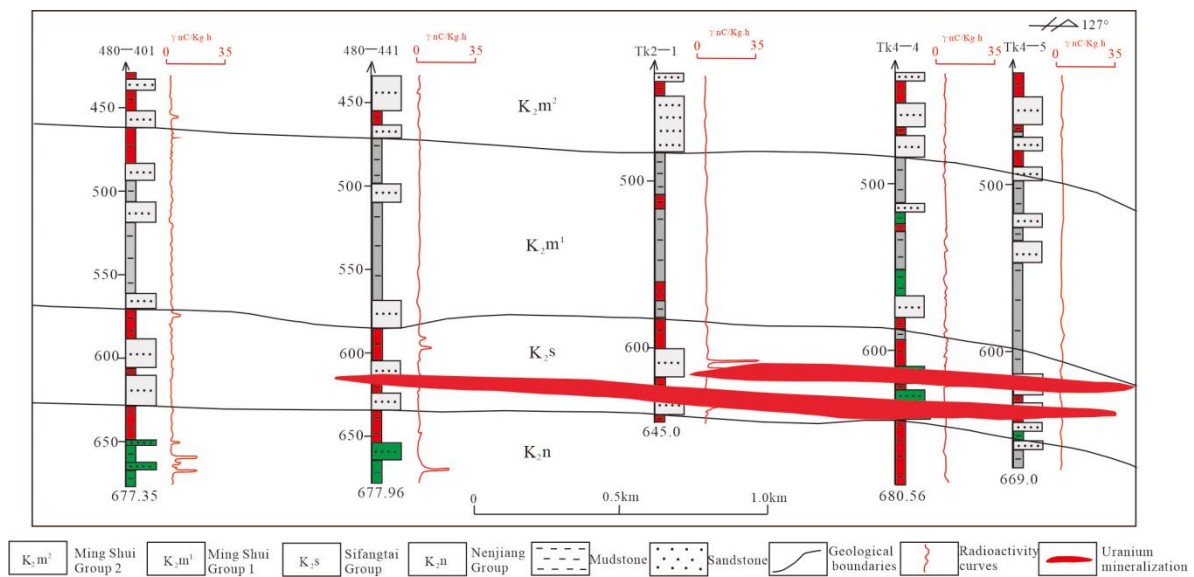


Figure 16. Uranium mineralization in the Sifangtai Formation, northern Songliao Basin.

The uranium mineralization sequence of events is as follows; (1) firstly, sandstones begin with the fluvial deposition of the arkose, then burial and lithification, (2) secondly, the uranium-bearing oxygenated water into some of the sandstone, nevertheless, the fracture development in the basin, a low temperature hydrocarbon transport of uranium through the faults into enriched portions of the formation that acted as reducing agents for the concentration of the uranium, and (3) finally, the sandstone is enriched in mineralization at the transition site (Figure 17).

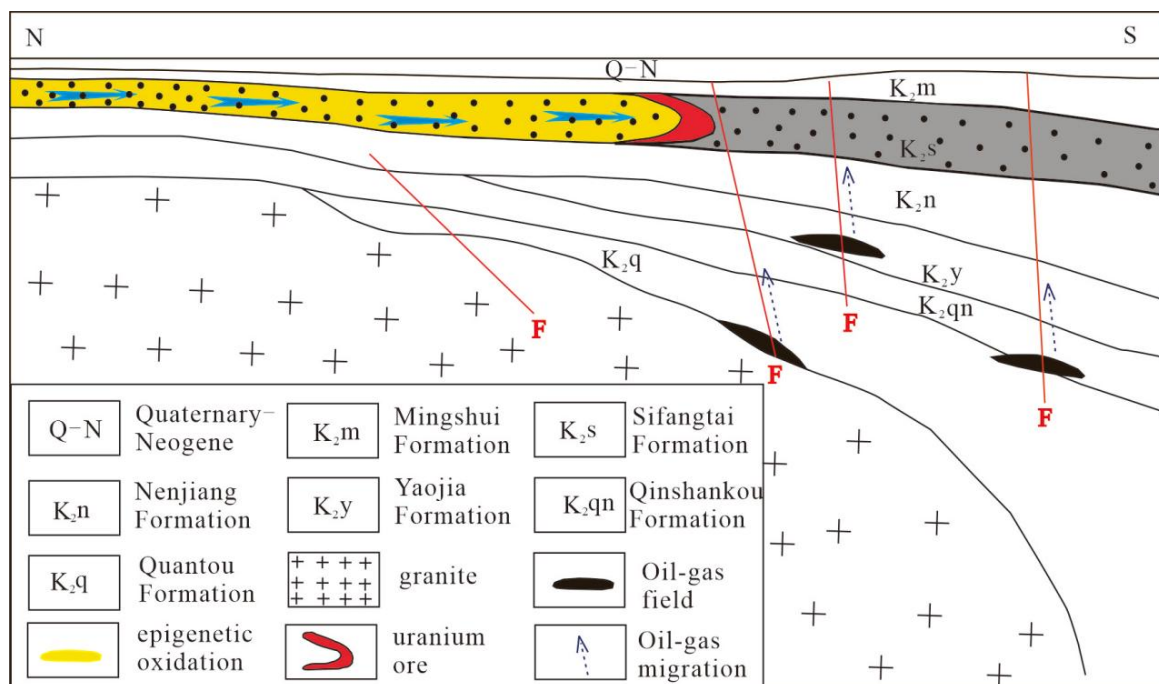


Figure 17. Uranium mineral model of the Sifangtai Formation in the northern part of the Songliao Basin.

In summary, the Sifangtai Formation in the northern region of the Songliao Basin is rich in uranium sources, tectonic conditions, ore-bearing favorable sand bodies, post-generation alteration, and paleoclimatic conditions, and it has considerable potential.

6. Conclusions

Based on the geochemistry of the sandstones in the northern Songliao Basin, in combination with the results of previous studies conducted in the area, we reached the following conclusions:

1. The ICV value ranged from 0.60 to 1.03, with an average of 0.69. The revised average CIA value was 54.35. It indicated that the rocks of the Sifangtai Formation might have undergone weak chemical weathering and the compositional homogeneity and minimal influence of sedimentary sorting.
2. The combination of element Sr/Ba, 100MgO/Al₂O₃ and the combination of $v/v + Ni$, V/Cr, Ni/Co, Sr/Cu indicated that the paleo-water medium was deposited in an oxygen-rich freshwater environment when the Sifangtai Formation was deposited.
3. On the structure discriminate diagrams, it showed that almost all the sandstones of the Sifangtai Formation fell in the range of active continental margin, indicating that the source area of the sandstones of Sifangtai Formations is an active continental margin tectonic environment, and the source is a felsic rock developed in the Xiaoxing'an Ridge and Zhangguangcailing area.
4. Diagrams of major (trace) elements reveal the paleoclimate of the source area and the warm arid climate prevails during the deposition period.
5. Based on the above comprehensive analyses, it was concluded that the paleo-climate, oxygen-rich paleo-water body, favorable sedimentary facies and thick sand bodies had important geological significance for the large-scaled mineralization of the sandstone-type uranium in the northern margin of the Songliao basin.

Author Contributions: Y.L., F.-J.N., L.-C.J., S.-J.L., Z.-B.Y., designed the project; Y.L. wrote and organized the paper, with a careful discussion and revision by F.-J.N., L.-C.J., S.-J.L., and Z.-B.Y. All authors have read and agreed to the published version of the manuscript.

Funding: This work was financially supported by China Nuclear Industry Geological Bureau (Grant No. 202125), Nuclear Energy Development Project of National Defense Bureau of Science and Industry (No. 20171403) and Fundamental Science on Radioactive Geology and Exploration Technology Laboratory, East China University of Technology (Grant No. 2020RGET02).

Institutional Review Board Statement: Not applicable.

Informed Consent Statement: Not applicable.

Data Availability Statement: The data presented in this study are available in this article.

Conflicts of Interest: The authors declare no conflict of interest.

References

1. Chen, Z.Y.; Chen, D.S.; Gu, K.H.; Wang, Y.J. The regional distribution of ore-bearing horizon, mineralization type and mineralization age of sandstone-type uranium deposits in China. *Uranium Geol.* **2010**, *26*, 321–330. (In Chinese with English abstract)
2. Nie, F.J.; Li, M.G.; Yan, Z.B.; Xia, F.; Zhang, C.Y.; Yang, J.X.; Kang, S.H.; Shen, K.F. Sublevel and Uranium Mineralization of Saihan Formation Target Layer of Sandstone-type Uranium Deposit in Erlian Basin, Inner Mongolia. *Geol. Bull. China* **2015**, *34*, 1952–1963. (In Chinese with English abstract)
3. Tang, C.; Wei, J.L.; Xiao, P.; Xu, Z.L.; Zeng, H.; Xu, L.L.; Guo, H.; Zhao, L.J. Study on occurrence state of uranium in sandstone-type uranium deposit in northern Songliao basin. *Miner. Resour. Geol.* **2017**, *32*, 1010–1016. (In Chinese with English abstract)
4. Zhang, J.D. Potential and evaluation of uranium resources in China. *Chin. Unclear Ind.* **2008**, *2*, 18–21. (In Chinese with English abstract)
5. Zhang, X.; Nie, F.J. Analysis of provenance of the uranium-bearing target layer and its tectonic setting in the Shihongtan uranium deposit Xinjiang: evidence from the petrology and geochemistry. *Sci. Technol. Eng.* **2019**, *19*, 86–92. (In Chinese with English abstract)
6. Xia, F.Y.; Jiao, Y.Q.; Rong, H.; Zhu, Q.; Wan, L.L. Geochemical Characteristics and Geological Implications of Sandstones from the Yaojia Formation in Qianjiadian Uranium Deposit, Southern Songliao Basin. *Earth Sci.* **2019**, *44*, 4236–4251. (In Chinese with English abstract)
7. Xu, Z.L.; Li, H.L.; Li, J.G.; Zhu, H.; Cao, M.Q.; Wei, J.L. Geochemistry of the Yaojia Formation Sandstone in the Kailu Depression, Songliao Basin: Implications for its Provenance and Tectonic Setting. *Bull. Mineral. Petrol. Geochem.* **2019**, *38*, 572–586. (In Chinese with English abstract)

8. Lu, C.; Peng, Y.B.; Liu, X.Y.; Jiao, Y.Q.; Yang, J.X.; Chen, F.Z.; Shen, K.F.; Li, R.L. Sedimentary background of sandstone-type uranium deposits in western margin depression of Erlian basin. *Uranium Geol.* **2013**, *29*, 336–343. (In Chinese with English abstract)
9. Wu, B.L.; Zhang, W.Y.; Song, Z.S.; Cun, X.N.; Sun, L.; Luo, J.J.; Li, Y.Q.; Cheng, X.H.; Sun, B. Geological and geochemical characteristics of uranium minerals in the sandstone-type uranium deposits in the north of Ordos basin and their genetic significance. *Acta Geol. Sin.* **2016**, *90*, 3393–3407. (In Chinese with English abstract)
10. Zhang, T.F.; Sun, L.X.; Zhang, Y.; Cheng, Y.H.; Li, Y.F.; Ma, H.L.; Lu, C. The geochemical characteristics of trace and rare earth elements in the mudstone of Yanan Formation and Zhuluo Formation in the northern margin of Ordos basin and their paleo-sedimentary environment significance. *Acta Geol. Sin.* **2016**, *90*, 3454–3472. (In Chinese with English abstract)
11. Yang, D.G.; Wu, J.H.; Nie, F.J.; Bonnetti, C.; Xia, F.; Yan, Z.B.; Cai, J.F.; Wang, C.D.; Wang, H.T. Petrogenetic Constraints of Early Cenozoic Mafic Rocks in the Southwest Songliao Basin, NE China: Implications for the Genesis of Sandstone-Hosted Qianjiadian Uranium Deposits. *Minerals* **2020**, *10*, 1014. [[CrossRef](#)]
12. Zhang, M.Y.; Zheng, J.W.; Tian, S.F.; Liu, H.B. Research on Existing State of Uranium and Uranium Ore-Formation Age at Qianjiadian Uranium Deposit in Kailu Depression. *Uranium Geol.* **2005**, *21*, 213–218. (In Chinese with English abstract)
13. Rong, H.; Jiao, Y.Q.; Wu, L.Q.; Ji, D.M.; Li, H.L.; Zhu, Q. Epigenetic alteration of qianjiadian uranium deposit in the south of Songliao basin and its constraint on uranium mineralization. *Earth Sci.* **2016**, *41*, 153–166. (In Chinese with English abstract)
14. Chen, F.H.; Zhang, M.Y.; Lin, C.S. The sedimentary environment of the Yaojia Formation and its uranium-rich significance in the Qianjiadian sag, Kailu basin. *Sediment. Tethys Geol.* **2005**, *25*, 74–79. (In Chinese with English abstract)
15. Chen, X.L.; Fang, X.X.; Guo, Q.Y.; Pang, Y.Q.; Sun, Y. A new understanding of uranium mineralization in Qianjiadian sag, Songliao basin. *Acta Geol. Sin.* **2008**, *82*, 553–561. (In Chinese with English abstract)
16. Xiao, P.; Tang, C.; Wei, J.L.; Xu, Z.L.; Zeng, H.; Liu, H.J. Sedimentary facies of the Sifangtai Formation in the southern Daqing anticline and its controls to uranium mineralization. *Geol. Surv. Res.* **2018**, *41*, 18–24. (In Chinese with English abstract)
17. Ma, H.F.; Luo, Y.; Li, Z.Y.; He, Z.B.; Wang, M.T. Sedimentary Features and Uranium Metallogenic Conditions of Yaojia Formation in Southern Songliao Basin. *Uranium Geol.* **2008**, *25*, 144–149. (In Chinese with English abstract)
18. Liu, X.Y. Prospecting Direction of Sandstone Type Uranium Deposits in Erlian Basin. *Uranium Geol.* **2021**, *01*, 51–60. (In Chinese with English abstract)
19. Li, J.; Gui, H.R.; Chen, L.W.; Fang, P.; Li, G.P.; Li, R.R. Geochemical characteristics, palaeoenvironment, and provenance of marine mudstone in Shanxi Formation of Huaibei Coalfield, southern North China Plate. *Geol. J.* **2021**, *56*, 3064–3080. [[CrossRef](#)]
20. Nebitt, H.W. Mobility and fraction of rare earth elements during weathering of a granodiorite. *Nature* **1979**, *279*, 206–210. [[CrossRef](#)]
21. McLennan, S.M.; Taylor, S.R. Sedimentary rocks and crustal evolution revisited: Tectonic setting and secular trends. *Geology* **1991**, *99*, 1–21. [[CrossRef](#)]
22. McLennan, S.M.; Hemming, S.R.; McDaniel, D.K. Geochemical approaches to sedimentation provenance and tectonics. In *Processes Controlling the Composition of Clastic Sediments*; Johnsson, M.J., Basu, A., Eds.; Geological Society of America, Inc.: Boulder, CO, USA, 1993; Volume 284, pp. 21–40.
23. Algeo, T.J.; Maynard, J.B. Trace element behavior and redox facies in core shales of upper Pennsylvanian Kansas type cyclothem. *Chem. Geol.* **2004**, *206*, 289–318. [[CrossRef](#)]
24. Algeo, T.J.; Tribouillard, N. Environmental analysis of paleoceanographic systems based on molybdenum uranium covariation. *Chem. Geol.* **2009**, *268*, 211–225. [[CrossRef](#)]
25. Calvert, S.E.; Pedersen, T.D. Geochemistry of recent oxic and anoxic marine sediments: implications for the geological record. *Mar. Geol.* **1993**, *113*, 67–88. [[CrossRef](#)]
26. Li, S.C.; Zhang, J.Y.; Gong, F.H.; Zhu, H.; Bai, Y.F. The characteristics of mudstones of Upper Cretaceous Qingshankou Formation and favorable area optimization of shale oil in the north of Songliao Basin. *Geol. Bull. China* **2017**, *36*, 654–663. (In Chinese with English abstract)
27. Liu, X.H.; Luo, M. Analysis on uranium metallogenic conditions and prospecting direction of Sifangtai Formation in TaiKang of Songliao Basin. *Geol. Resour.* **2021**, *30*, 14–20. (In Chinese with English abstract)
28. Dai, W.Y.; Li, Y.; Zhao, Z.H.; Zhang, Y.; Zhang, H. Exploration on metallogenic conditions and prospecting direction of Jurassic sandstone type uranium deposit in Northeast margin of Songliao basin. *Geol. Resour.* **2019**, *28*, 519–526. (In Chinese with English abstract)
29. Zhou, J.B.; Zhang, X.Z.; Ma, Z.H. Tectonic framework and basin evolution in Northeast China. *Oil Gas Geol.* **2009**, *30*, 530–538.
30. Liu, J.L.; Qin, M.K.; Cai, Y.Q.; Liu, Z.Y.; Zhang, Z.M.; Yao, L. Late Mesozoic tectonic evolution of the southern Great Xing'an Range, northeastern China: Constraints from detrital zircon U–Pb and Hf isotopes of Late Cretaceous sandstones in the southwestern Songliao Basin. *Geol. J.* **2020**, *55*, 4415–4425. [[CrossRef](#)]
31. Feng, Z.Q.; Zhang, S.; Fu, X.L. Sedimentary evolution and accumulation response of Yaojia Formation and Nenjiang Formation in Songliao basin. *Earth Sci. Front.* **2012**, *19*, 78–87. (In Chinese with English abstract)
32. Jiao, Y.Q.; Wu, L.Q.; Peng, Y.B. Sedimentary-tectonic setting of the deposition type uranium deposits forming in the Paleo-Asian tectonic domain, North China. *Earth Sci. Front.* **2015**, *22*, 189–205.
33. Li, J.; Huang, Z.L.; Li, L.J.; Liu, B.Z. A new understanding of uplift process in the southeastern uplift area of Songliao basin. *Xinjiang Pet. Geol.* **2008**, *29*, 690–692. (In Chinese with English abstract)

34. Shi, S.S.; Ren, J.Y.; Zhang, S.; Fu, X.L.; Tang, S.M. Sequence Stratigraphic Framework and its foemation mechanism of Post~Rift inversion successin in North of Songliao Basin, China. *Earth Sci.-J. Univ. Geosci.* **2012**, *37*, 545–555. (In Chinese with English abstract)
35. Sun, Y.H.; Bai, L.; Fu, X. Genetic mechanism of T2 reflector fault density belt in northern Songliao basin. *Earth Sci.* **2013**, *38*, 797–805. (In Chinese with English abstract)
36. Song, Y.; Ren, J.Y.; Yang, H.Z.; Tong, J.J.; Lei, C. Characteristics and dynamic background of bottom boundary in Yaojia Formation of the northern Songliao Basin. *Acta Petrol. Sin.* **2010**, *31*, 187–195. (In Chinese with English abstract)
37. Chen, F.K.; Siebel, W.; Satir, M. Geochronology of the Karadere basement (N W T urkey) and implications for the geological evolution of the Istanbul zone. *Int. J. Earth Sci.* **2002**, *91*, 469–481. [[CrossRef](#)]
38. Herron, M.M. Geochemical classification of terrigenous sands and shales from core or log data. *J. Sediment. Petrol.* **1998**, *58*, 820–829. [[CrossRef](#)]
39. Sun, S.S.; McDonough, W.F. Chemical and isotopic systematics of oceanic basalts: Implications for mantle composition and processes. In *Magmatism in Ocean Basins*; Saunders, A.D., Norry, M.J., Eds.; Geological Society of Special Publication: London, UK, 1989; Volume 27, pp. 313–345.
40. Cox, R.; Lowe, D.R.; Cullers, R.L. The infuence of sediment recyling and basement composition on evolution of mudrock chemistry in the south western United States. *Geochim. Cosmochim. Acta* **1995**, *59*, 2919–2940. [[CrossRef](#)]
41. Cullers, R.L.; Podkovyrov, V.N. Geochemistry of the Mesoproterozoic Lakhanda shales in southeastern Yakutia, Russia: Implications for mineralogical and provenance control, and recycling. *Precambrian Res.* **2000**, *104*, 77–93. [[CrossRef](#)]
42. Fathy, D.; Wagreich, M.; Zaki, R.; Mohamed, R.S.A.; Gier, S. Geochemical fingerprinting of Maastrichtian oil shales from the Central Eastern Desert, Egypt: Implications for provenance, tectonic setting, and source area weathering. *Geol. J.* **2018**, *53*, 2597–2612. [[CrossRef](#)]
43. Nesbitt, H.W.; Young, G.M. Early Proterozoic climates and plate motions inferred from major element chemistry of lutites. *Nature* **1982**, *299*, 715–717. [[CrossRef](#)]
44. Nesbitt, H.W.; Young, G.M. Prediction of some weathering trends of plutonic and volcanic rocks based on thermodynamic and kinetic considerations. *Geochim. Cosmochim. Acta* **1984**, *48*, 1523–1534. [[CrossRef](#)]
45. Fedo, C.M.; Nesbitt, H.W.; Young, G.M. Unraveling the effects of potassium metasomatism in sedimentary rocks and paleosols, with implications for paleoweathering conditions and povenance. *Geology* **1995**, *23*, 921–924. [[CrossRef](#)]
46. Kasanzu, C.; Maboko, M.A.H.; Many, S. Geochemistry of finegrained clastic sedimentary rocks of the Neoproterozoic Ikorongo Group, NE Tanzania: Implications for provenance and source rock weathering. *Precambrian Res.* **2008**, *164*, 201–213. [[CrossRef](#)]
47. Deng, H.W.; Qian, K. *Sedimentary Geochemistary and Environmental Analysis*; Gansu Science and Technology Press: Lanzhou, China, 1994; pp. 1–154.
48. Jones, B.; Manning, D.A.C. Comparion of geochemical indices used for the interpretation of palaeoredox conditions in ancient mudstones. *Chem. Geol.* **1994**, *111*, 111–129. [[CrossRef](#)]
49. Lermanm, A. *Lakes: Chemistry, Geology, Physics*; Lerman, A., Ed.; Springer: Berlin, Germany, 1978; pp. 79–83.
50. Tribovillard, N.; Algeo, T.J.; Lyons, T. Trace metals as paleoredox and paleoproductivity proxies: Anudate. *Chem. Geol.* **2006**, *232*, 12–32. [[CrossRef](#)]
51. Schieber, J.A. Combined petrographical-geochemical provenance study of the Newland Formation, Mid-Proterozoic of Montana. *Geol. Mag.* **1992**, *129*, 223–237. [[CrossRef](#)]
52. Hayashi, K.I.; Fujisawa, H.; Holland, H.D. Geochemistry of ~1.9Ga sedimentary rocks from northeastern Labrador, Canada. *Geochim. Cosmochim. Acta* **1997**, *61*, 4115–4137. [[CrossRef](#)]
53. Floyd, P.; Leveridge, B.E. Tectonic environment of the Devonian Gramscatho basin, south Cornwall: Framework mode and geochemical evidence from turbiditic sandstones. *J. Geol. Soc.* **1987**, *144*, 531–540. [[CrossRef](#)]
54. Floyd, P.A.; Winchester, J.A.; Park, R.G. Geochemistry and tectonic setting of Lewisian clastic metasediments from the Early Proterozoic Loch Maree Group of Gairloch, NW Scotland. *Precambrian Res.* **1989**, *45*, 203–214. [[CrossRef](#)]
55. Bhatia, M.R.; Crook, K.A.W. Trace element characteristics of graywackes and tectonic setting discrimination of sedimentary basins. *Mineral. Petrol.* **1986**, *92*, 181–193. [[CrossRef](#)]
56. Wu, F.Y.; Sun, D.Y.; Li, H.M.; Jahn, B.M.; Wilde, S.A. A-type granites in northeastern China: Age and geochemical constraints on their petrogenesis. *Chem. Geol.* **2002**, *187*, 143–173. [[CrossRef](#)]
57. Wu, F.Y.; Jahn, B.M.; Wilde, S.A.; Lo, C.H.; Yui, T.F.; Lin, Q.; Ge, W.C.; Sun, D.Y. Highly fractionated I- type granites in NE China(I): Geochronology and petrogenesis. *Lithos* **2003**, *66*, 241–273. [[CrossRef](#)]
58. Liu, W.; Siebel, W.; Li, X.J.; Pan, X.F. Petrogenesis of the Linxi granitoids, northern Inner Mongolia of China: Constraints on basaltic underplating. *Chem. Geol.* **2005**, *219*, 5–35. [[CrossRef](#)]
59. Ge, W.C.; Wu, F.Y.; Zhou, C.Y.; Zhang, J.H. Porphyry Cu-Mo deposits in the eastern Xing-an—Mongolian orogenic belt: Mineralization ages and their geodynamic implications. *Chin. Sci. Bull.* **2007**, *52*, 3416–3427. [[CrossRef](#)]
60. Zhang, J.H. Study on the Chronology and Geochemistry of Mesozoic Volcanic Rocks in Daxing’an Mountains. Doctoral Dissertation, China University of Geosciences, Wuhan, China, 2009; pp. 36–49. (In Chinese with English abstract)
61. Zhang, Y.L.; Ge, W.C.; Gao, Y. U-Pb age, Hf isotope and geological significance of granite zircons in longzhen area. *Acta Petrol. Sin.* **2010**, *26*, 1059–1073. (In Chinese with English abstract) [[CrossRef](#)]
62. Zong, M.S.; Wang, Z.J.; Ao, G. Zircon U-Pb chronology and geochemical characteristics of igneous rocks in Erlanghe Formation, Zhang Guangcai Ridge, China. *Geol. Surv. Res.* **2017**, *40*, 161–168. (In Chinese with English abstract)

63. Zhao, B.; Wang, C.S.; Wang, X.F. Late Cretaceous (Campanian) provenance change in the Songliao Basin, NE China: Evidence from detrital zircon U—Pb ages from the Yaojia and Nenjiang formations. *Palaeogeogr. Palaeoclimatol. Palaeoecol.* **2013**, *385*, 83–94. [[CrossRef](#)]
64. Li, S.Q.; Chen, F.K.; Siebel, W. Late Mesozoic tectonic evolution of the Songliao Basin, NE China: Evidence from detrital zircon ages and Sr—Nd isotopes. *Gondwana Res.* **2012**, *22*, 943–955. [[CrossRef](#)]
65. Gao, Y.F.; Wang, P.J.; Qu, X.J. Sedimentary facies and cyclostratigraphy of the Cretaceous first member of Nenjiang Formation in the southeast uplift zone, Songliao Basin and its correlation with the CCSD-SK-I. *Acta Petrol. Sin.* **2010**, *26*, 99–108. (In Chinese with English abstract)
66. Chen, R.H.; Wang, G.d.; Wang, P.J. Upper-most Cretaceous sediments: Sedimentary microfacies and sedimentary environment evolution of Sifangtai Formation and Ming-shui Formation in SK-I. *Earth Sci. Front.* **2009**, *16*, 85–95. (In Chinese with English abstract)
67. Feng, Z.Q.; Jia, C.Z.; Xie, X.N. Tectonostratigraphic units and stratigraphic sequences of the nonmarine Songliao Basin, northeast China. *Basin Res.* **2010**, *22*, 79–95.
68. Xiao, P.; Jin, R.S.; Tang, C.; Liu, H.J.; Deng, Y.H.; Wei, J.L.; Xu, Z.L. Provenance system of the Late Cretaceous Sifangtai Formation in the south of Daqing placanticline of the northern Songliao Basin. *Pet. Geol. Exp.* **2018**, *44*, 493–501, (in Chinese with English abstract).
69. Roser, B.P.; Korsch, R.J. Provenance Signatures of Sandstone-Mudstone Suites Determined Using Discriminant Function Analysis of Major-Element Data. *Chemical Geol.* **1988**, *67*, 119–139. [[CrossRef](#)]
70. Maynard, J.B.; Valloni, R.; Yu, H.S. Composition of modern deep-sea sands from arc-related basins. In *Trench and Fore-Arc Sedimentation*; Leggett, J.K., Ed.; Geological Society of London Special Publications: London, UK, 1982; Volume 10, pp. 551–561.
71. Bhatia, M.R. Plate tectonics and geochemical composition of sandstones. *J. Geol.* **1983**, *91*, 611–627. [[CrossRef](#)]
72. Yang, Y.C.; Han, S.J.; Sun, D.Y. Geological and geochemical features and geochronology of porphyry molybdenum deposits in the Lesser Xing’an Range-Zhangguangcai Range metallogenic belt. *Acta Petrol. Sin.* **2012**, *28*, 379–390. (In Chinese with English abstract)
73. Liu, Y.J.; Zhang, X.Z.; Jin, W.; Chi, X.G.; Ma, Z.H. Late Paleozoic regional tectonic evolution in northeast China. *Geol. China* **2010**, *37*, 943–951. (In Chinese with English abstract)
74. Li, B.L.; Song, Y.G.; Chen, G.J.; Xi, A.L.; Zhi, Y.B.; Chang, J.J.; Peng, B. Zircon U-Pb Geochronology, Geochemistry and Hf Isotopic Composition and its geological implication of the Fine-Grained syenogranite in Dongan gold field from the Lesser Xingan Mountains. *Earth Sci.* **2016**, *41*, 1–16. (In Chinese with English abstract)
75. Ge, M.H.; Zhang, J.J.; Liu, K.; Wang, M.; Li, Z. Petrogenesis of the Late Paleozoic to Mesozoic granite from the Xiao Hinggan Mountains-Zhangguangcai Mountains and its geological implications. *Acta Petrol. Mineral.* **2020**, *39*, 385–405.
76. Zhao, Y.; Liu, J.D.; Zhang, G.B.; Zhang, G.B. Geochronology, geochemistry and tectonic significance of the Monzonitic granites of Maoershan pluton from the southern Zhangguangcailing in Heilongjiang Province, China. *J. Jilin Univ. (Earth Sci. Ed.)* **2021**, *51*, 1098–1117.
77. Zhao, Z.H.; Bai, J.P.; Lai, T.G. Inversion structure and sandstone-type uranium mineralization in northern songliao basin. *Uranium Geol.* **2018**, *34*, 292–297. (In Chinese with English abstract)
78. He, Z.B.; Ji, H.L.; Wei, S.Y.; Cao, J.H.; Lin, X.B. Discussion on Prospecting Direction of Sandstone Type Uranium Deposits in Sanjiang Basin, Heilongjiang Province. *J. Jilin Univ. (Earth Sci. Ed.)* **2019**, *51*, 367–379. (In Chinese with English abstract)